FACULTY OF SCIENCES

Center for Molecular and Vascular Biology

Department of Cardiovascular Sciences
Centre for Molecular and Vascular Biology

HEART FAILURE WITH PRESERVED EJECTION FRACTION – A COMPARISON OF ANIMAL MODELS AND THE ROLE OF ENDOTHELIAL PITX2 LOSS

Jana Raman
Student number: 01508173

Supervisor(s): Prof. Dr. Elizabeth Jones (KU Leuven)
Prof. Dr. Bart P. Braeckman

Scientific tutor: Dr. Steven Simmonds (KU Leuven)

Master's dissertation submitted to obtain the degree of Master of Science in Biology

Academic year: 2019 - 2020

GHENT UNIVERSITY

KU LEUVEN

Table of Contents

1 LIST OF ABBREVIATIONS

A	Late mitral inflow blood peak velocity
A’	Late diastolic mitral annulus peak velocity
BNP	Brain natriuretic peptide
Col	Collagen
DAB	3,3'-diaminobenzidine
DAPI	4',6-diamidino-2-fenylindool
DPX	Distrene plasticizer xylene
DT	Deceleration time
E	Early mitral inflow blood peak velocity
E’	Early diastolic mitral annulus peak velocity
ECM	Extracellular matrix
EF	Ejection fraction
HA	Hyaluronan
HF	Heart Failure
HFD	High Fat Diet
HFpEF	Heart Failure with preserved Ejection Fraction
HFrEF	Heart Failure with reduces Ejection Fraction
HRP	Horse Radish Peroxidase
IB_4	Isolectin B_4
IGF-1	Insulin-like Growth Factor 1
IHC	Immunohistochemistry
IL-6	Interleukin 6
IVRT	Isovolumetric relaxation time
L-NAME	Nω-nitro-l-arginine methyl ester hydrochloride
LOX	Lysyl oxidase
LV	Left ventricle
LVIDd	Left ventricular internal dimension at end-diastole
MeOH	Methanol
NADPH	Nicotinamide adenine dinucleotide phosphate oxidase
NO	Nitric oxide
NOS	Nitric oxide synthase
PBS	Phosphate-buffered Saline
PBT	Phosphate-buffered saline with triton
PDGF	Platelet derived growth factor (PDGF)
PFA	Paraformaldehyde
Pitx2	Paired-like homeodomain transcription factor 2
PKG	Protein kinase G
PW	Pulsed wave
ROS	Reactive oxygen species
RT	Room temperature
T2DM	Type 2 diabetes mellitus
TAM	Tamoxifen

TBS	Tris-buffered saline
TGF-β	Transforming growth factor β1
TNB	Tris-NaCl-blocking
TNF-α	Tumour necrosis factor α
TNT	Tris-NaCl-tween buffer
TSG-6	Tumour necrosis factor-inducible gene 6
VEGF	Vascular endothelial growth factor

2 ABSTRACT

More than half of heart failure patients are diagnosed with Heart Failure with a preserved Ejection Fraction (HFpEF), a clinical syndrome characterized by cardiomyocyte stiffening, cardiac fibrosis, hypertrophy, and inflammation, which promote the development of diastolic dysfunction. HFpEF patients suffer from exercise intolerance, pulmonary congestion, peripheral oedema, and encounter high mortality rates. Increasingly, HFpEF is being characterised as a systemic progressive syndrome, that starts from peripheral risk factors and culminates in heart failure. Typical associated comorbidities, such as increased age, obesity, type 2 diabetes, hypertension, and kidney disease, are hypothesised to drive HFpEF development by exposing endothelial cells to systemic inflammation and oxidative stress.

The exact pathogenesis of HFpEF remains unelucidated, and our understanding of disease is further impeded by the absence of appropriate animal models that accurately mimic the complex heterogeneity in disease presentation by different patient cohorts. The first objective of this thesis project is to compare two existing mouse models (aged mice and *db/db* salt treated mice) and one recently published HFpEF model (high fat diet and L-NAME treated mice; HFD + L-NAME) upon different HFpEF features.

Additionally, our preliminary data indicate that endothelial-specific loss of paired-like homeodomain transcription factor 2 (Pitx2) expression may drive vessel regression and HFpEF progression. Therefore, the second aim is to investigate the occurrence of coronary microvascular rarefaction, in a conditional inducible *Pitx2*^{ECKO} mouse. To achieve this all, animals were examined for changes in morphometry, cardiac function using echocardiography, and cardiac remodelling via histological techniques.

We demonstrate that *db/db* mice given a salt treatment most accurately recapitulate the human HFpEF phenotype. These mice were the only model with obesity and the advanced, restrictive stage of diastolic dysfunction, coupled to coronary capillary rarefaction and cardiomyocyte enlargement. The salt diet thus accelerated diastolic dysfunction development, compared to untreated *db/db* mice. HFD + L-NAME treated mice exhibited a pre-restrictive stage of diastolic dysfunction and the mild form of cardiac remodelling, which corresponded less to the HFpEF phenotype than expected. Of all models tested, the aged mice demonstrated the mildest stage of diastolic dysfunction, accompanied by increased fibrosis. However, the observed pseudonormal phase of diastolic dysfunction was still more severe compared to aging models specifically selected for their age-related abnormalities. We propose a concept in which the aging process functions as the backbone of HFpEF pathogenesis. In healthy conditions, the lifespan is too short, and the aging process cannot act long enough on the heart. However, when triggered by metabolic or mechanical stress in the form of comorbidities, cardiac aging gets stimulated and results in more advanced cardiac remodelling and diastolic dysfunction.

Endothelial Pitx2 deficiency resulted in systolic dysfunction rather than diastolic dysfunction and a reduction in coronary microvascular density, uncoupled of cardiomyocyte enlargement. A second experiment where Pitx2 is only conditionally deleted upon adulthood in *Pitx2*^{ECKO} mice, is ongoing.

The variation between our different comorbidity models, and the heterogeneity found in HFpEF patients highlight the need for multiple appropriate animal models to further understand this complex disease.

3 INTRODUCTION

3.1 Heart Failure with preserved Ejection Fraction

The healthy heart is a strong muscular organ that pumps blood continuously through the circulatory system, providing the body with oxygen and nutrients. The cardiac cycle is divided into diastole and systole. Diastole represents ventricular filling, while systole represents ventricular contraction and subsequent blood ejection into the aorta. Diastole begins at the closing of the aortic valve, between the left ventricle (LV) and the aorta. The LV relaxes, fills with blood, and the closing of the mitral valve, between the left atrium and the LV, terminates diastole. Systole starts when the mitral valve closes. The pressure within the ventricles becomes greater than adjacent aorta and blood will be directed outwards. Systole ends with the closure of the aortic valve [1].

Heart failure (HF) is a clinical syndrome in which the capacity of the heart is unable to meet the required cardiac output, defined as the amount of blood ejected per minute, to meet the body's metabolic needs [2]. As the heart attempts to maintain adequate cardiac output levels, several compensatory mechanisms are initiated. In early stages, these measures are beneficial, as they superficially promote physiological functioning, however, on the long term, they gradually worsen the vicious circle of heart failure. Patients develop several clinical symptoms, including tachycardia, dyspnea from pulmonary congestion, peripheral oedema, nausea, exercise intolerance, and fatigue [2]. HF is responsible for 1-3% of the total healthcare costs in the USA, Europe, and Latin America and causes the largest proportion of hospitalisations in Europe [3]. While HFpEF emerges rapidly as a clinical problem and no effective treatments are available [4].

More than half of the HF patients are diagnosed with Heart Failure with a preserved Ejection Fraction (HFpEF). HFpEF is a pathological condition characterized by cardiac stiffening, fibrosis, hypertrophy and inflammation [5]. Consequentially, the heart encounters reduced compliance and impaired blood filling of the LV during diastole and thus develops 'diastolic dysfunction'. This results in a decreased LV blood volume at end-diastole, so that less blood is ejected into the aorta at systole. This volume of ejected blood is referred to as the stroke volume. The ratio of stroke volume over end-diastolic volume in the LV defines the Ejection Fraction (EF) (**Figure 1**). HFpEF patients display a 'preserved' EF as both volumes are diminished [6].

Besides HFpEF, HF patients can also suffer from Heart Failure with reduced Ejection Fraction (HFrEF). In the heart of HFrEF patients, only the stroke volume reduces, resulting in a reduced EF (**Figure 1**) [2]. Either ischemia, infection, toxicity, or a combination of these induces a substantial cellular oxidative stress upon cardiomyocytes. These cardiomyocytes undergo necrosis, apoptosis, and autophagy, which results in the typical eccentric hypertrophy in HFrEF patients. Dead cardiomyocytes are replaced by collagen, thereby creating patchy areas of fibrosis [7]. Together, this LV remodelling causes the systolic dysfunction that characterises the HFrEF disease. Thus, HFrEF initiates from the heart as cardiac-centred pathology causing peripheral changes.

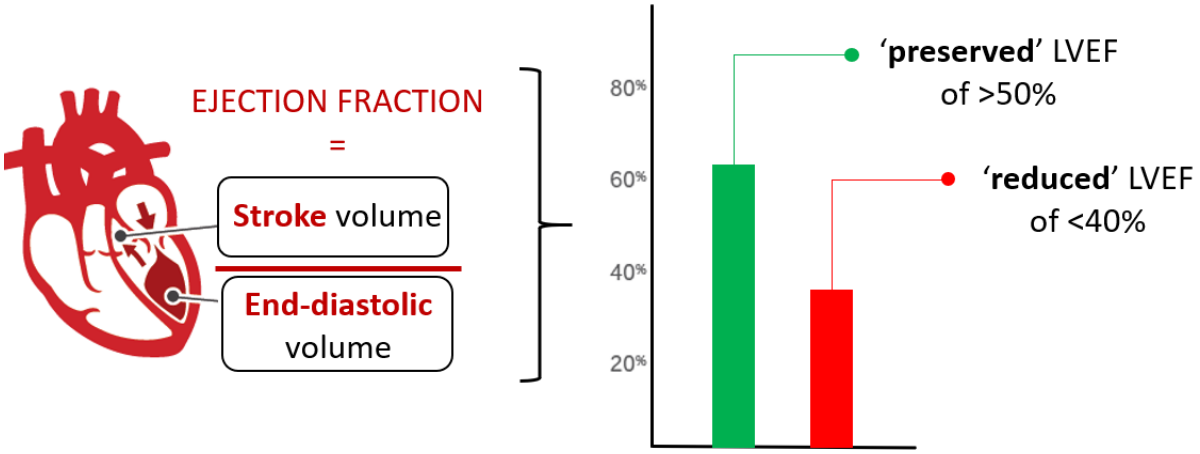

Figure 1: Defining 'preserved' and 'reduced' left ventricular ejection fraction (LVEF). The EF is defined by the ratio between stroke volume ejected into the aorta at systole, and the end-diastolic volume of the filled left ventricle. An EF lower than 40% is generally acknowledged to be 'reduced'. In HFpEF both the end-diastolic and therefore also the stroke volume diminish, resulting in a preserved EF above 50%. EF = ejection fraction. Adapted from Wilcox *et al*. 2012 [8].

In contrast to the cardiac-centred HFrEF, HFpEF is increasingly being defined as a systemic progressive syndrome that starts with peripheral changes driven by comorbidities that progresses in heart failure [9], [10]. Initially, HFpEF was thought to be the result of an increased afterload on the LV due to arterial hypertension [10]. However, HFpEF is more and more seen as a systemic disease, originating from a systemic inflammatory state [10]. HFpEF is typically associated with multiple risk factors and comorbidities that severely affect disease outcome. These include increased age (64-80 years), obesity (41-62%), Type 2 diabetes mellitus (T2DM; 26-45%), hypertension (55-86%), kidney disease (9-48%), and chronic obstructive pulmonary disease (COPD; 7-31%) [11][12]. Moreover, HFpEF is represented by an almost two-fold higher prevalence in women than in men [13]. This cluster of HFpEF comorbidities induce systemic inflammation and result in increased plasma levels of interleukin 6 (IL-6) and tumour necrosis factor α (TNF-α), and cause coronary endothelial dysfunction and ultimately to diastolic dysfunction [10]. As a consequence of the aging population and improved survival of patients with comorbidities, the incidence of HFpEF is increasing at an alarming rate and is expected to rise even further [14]. Importantly, the presence and severity of these comorbidities have great impact on clinical outcome of HFpEF patients [15]. Almost all comorbidities, expect hypertension, independently elevate patient mortality, with COPD being the best predictor [16]–[18]. Overall, short-term mortality (30-90 days) in the peri-hospitalisation period typically ranges between 5 and 9.5%, while long term (5 years) mortality rates are consistently high and varying from 55 to 74% [12]. The adverse link between HFpEF prognosis and its comorbidities increasingly advocates to perceive the comorbidities as drivers of HFpEF development, and to target them in HFpEF treatment [16].

Measuring changes in cardiac function through echocardiography

HFpEF is a condition that requires the combination of several echocardiography techniques for its diagnosis. Using echocardiography, typical functional parameters can be observed, such as EF and stroke volume. EF and stroke volume are informative haemodynamic parameters for systolic function, which can be assessed using M-mode imaging of the myocardial movement [4]. While HF is classified based on the EF, this value alone lacks efficacy in the diagnosis HFpEF, as patients exhibit a preserved EF [4]. Despite

this shortcoming, historical studies often only investigated this parameter, complicating the available literature.

In echocardiography, the M-mode imaging allows for accurate and real-time measurements of wall dimensions (thickness and diameters at systole and diastole) and heart rate. From these parameters many systolic and hypertrophy parameters can be derived (**Figure 2A**). At end-diastole, the LV Internal Diameter (LVIDd) and the LV Posterior Wall Thickness (LVPWd) can be measured using M-Mode imaging and together with the Relative Wall thickness (RWT) allow for the evaluation of LV hypertrophy and dilatation [19]. Increased RWT then indicates a hypertrophy of the wall in the LV.

To diagnose diastolic dysfunction, pulsed waved (PW) and tissue Doppler are used for assessing blood flow and myocardial velocity respectively (**Figure 2B)**. PW and tissue Doppler use the Doppler principle, where moving objects change the characteristic of sound waves. By sending short and quick pulses of sound, it allows the accurate measurement of the blood (PW Doppler) or myocardial wall (tissue Doppler) velocity at a precise location and in real time. Estimates of blood and myocardial wall flow velocity are subsequently calculated by comparing the frequency change between the transmitted and reflected sound waves, whereby an increase in Doppler shift indicates an increased blood flow velocity and vice versa.

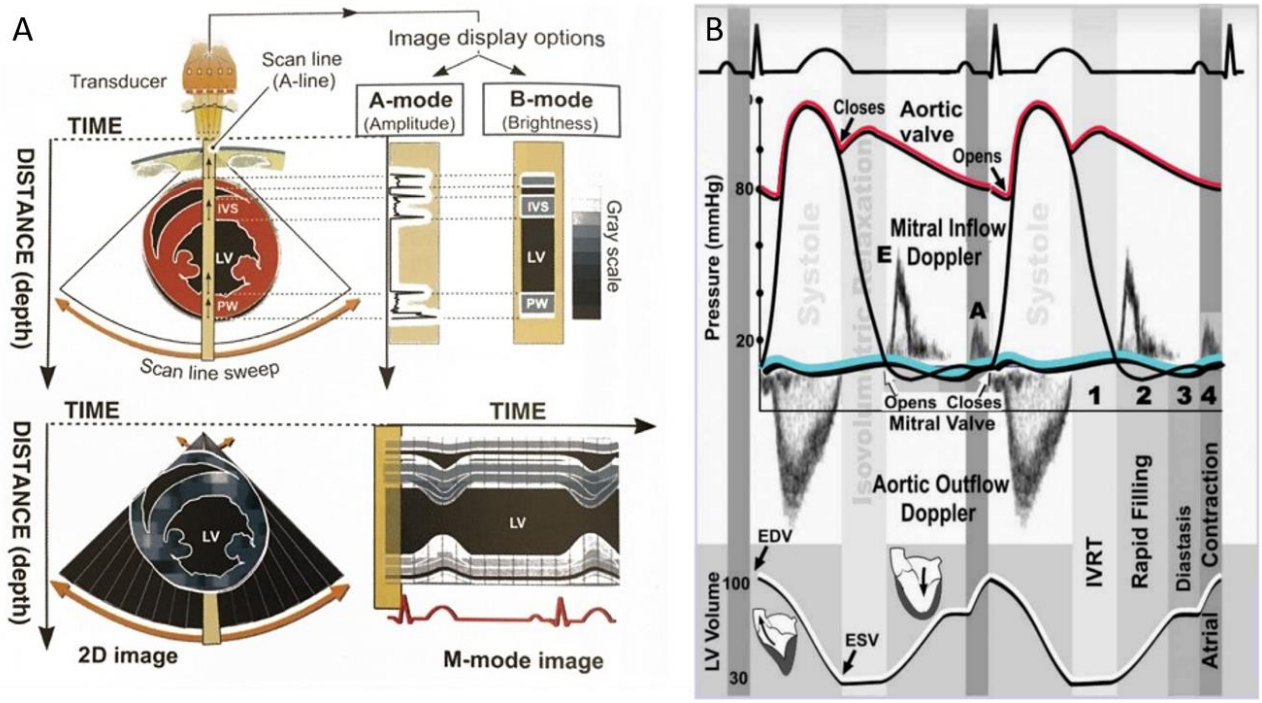

Figure 2: Different echocardiographic imaging modalities (A) M-mode imaging. **(B)** Cardiac cycle with pulsed wave Doppler imaging and electrocardiogram. The first phase of diastole, the isovolumic ventricular relaxation time (IVRT), comprises the left ventricular filling from the closure of the aortic valve until the opening of the mitral valve. Blood flows then passively from the left atrium in the ventricle (rapid passive filling) with an early mitral inflow peak velocity (E). During diastasis, active left ventricular relaxation is completed. During arterial systole, the left atrium contracts to accelerate the blood flow from the left atrium to the ventricle. The peak velocity of blood during this period is called the arterial or "late" mitral inflow peak velocity (A). EDV, end-diastolic volume; ESV, end-systolic volume. Left: from Braunwald's Heart disease. 2018 [20]. Right: from Ho C.Y. 2007 [21].

The four distinct phases of diastole can be assessed by Doppler imaging (**Figure 2B**). In the healthy heart, the isovolumic relaxation time (IVRT) starts at the closure of the aortic valve (end-systole) and ends at the opening of the mitral valve (start of diastole), representing an interval where the LV is a closed relaxed chamber. The IVRT can be measured by PW doppler. When the pressure in the LV falls below the pressure in the left atrium, leading to the opening of the mitral valve. Blood flows passively from the left atrium to the left ventricle (rapid passive filling). Both the peak velocities of blood flow during early filling (E) and the time from the E peak to the reach baseline velocity, called deceleration time (DT), can be measured by PW Doppler. The velocity of the cardiac muscle during this early filling phase, early diastolic mitral annulus peak velocity (E'), can be measured by tissue Doppler. During the third phase, diastasis, active left ventricular relaxation is completed, and the left ventricle slowly fills. This phase can be assessed both by PW and tissue Doppler. During the last phase of diastole, the atrial kick, the left atrium contracts, accelerating blood flow from the left atrium to the ventricle. The A peak velocity of blood (late mitral inflow velocity) and A' peak of cardiac movement (late diastolic mitral annulus peak velocity) can be assessed by PW and tissue Doppler respectively. Alterations of any of these diastolic phases leads to diastolic dysfunction [1].

Aforementioned diastolic measurements are the best echocardiographic markers to categorise the grade of diastolic dysfunction (**Figure 3**) [22]. In the healthy human heart, the E and E' peaks are higher than the A and A' peak respectively, inducing an E/A ratio between 1 and 2. Short DT and IVRT together with the unchanged E/E' ratio indicate preserved blood flow and relaxation of the LV during passive filling (**Figure 3**). Based on the parameters in this normal situation, diastolic dysfunction can be subdivided into 3 phases.

During the first, 'impaired relaxation stage', the LV shows reduced diastolic relaxation capacity in terms of compliance and elastic recoil, resulting in a slower LV pressure decline. Subsequently, it takes more time before the LV pressure equals the left atrial pressure, prolonging the IVRT. Due to the decreased relaxation, the LV passive filling occurs at lower velocities (E peak decreases), the filling-time extends (DT increases) and the A velocity is increased. As such, the atrial contraction compensates for the decrease in early filling, resulting in an E/A <1. As both early peak blood flow and muscle velocity are reduced, E/E' remains unchanged (**Figure 3**). Secondly, at the 'pseudonormal stage', progressive diastolic dysfunction causes the left atrial pressure to rise, driving the force to fill the LV at early diastole, leading to increased E velocities. However, while E increases, A decreases due to stiffening of the wall, resulting in a pseudonormal E/A. However, the E/E' ratio is severely increased due to reduced muscle relaxation (E') (**Figure 3**). Finally, during the 'restriction stage', the E/E' ratio rises further due the reduced E' and increased filling at early diastole (E) (**Figure 3**) [23].

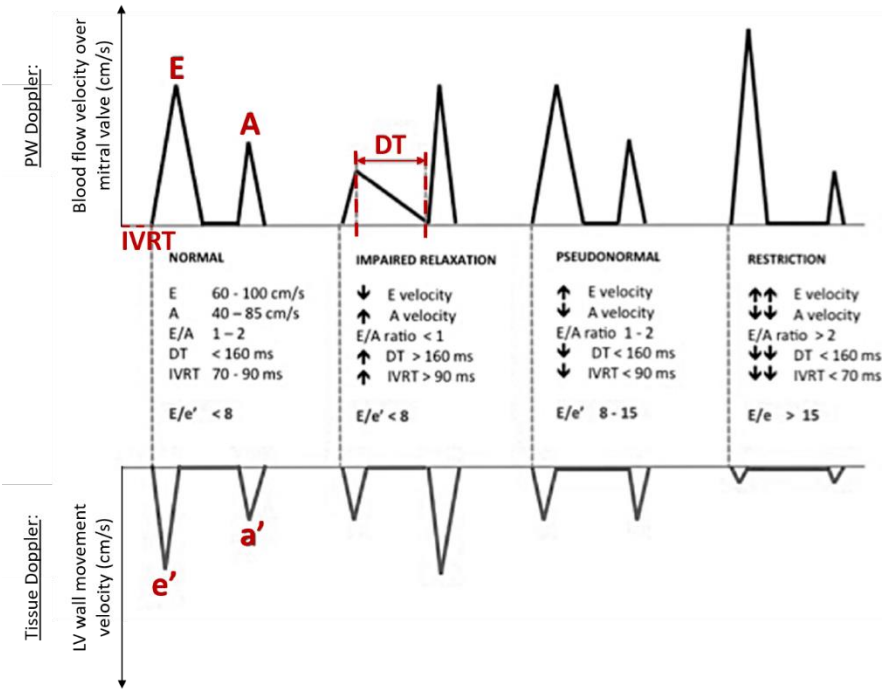

Figure 3. Theoretical filling patterns of 4 stage of diastolic dysfunction. Pulsed Wave Doppler and Tissue Doppler Imaging during the (1) normal, (2) impaired relaxation, (3) pseudonormal and (4) restriction stage of diastolic dysfunction. E = early mitral inflow blood peak velocity. A = Late mitral inflow blood peak velocity. DT = Deceleration time. IVRT = Isovolumetric relaxation time. e' = early diastolic mitral annulus peak velocity. a' = late diastolic mitral annulus peak velocity. Adapted from Vermeiren, *et al.*, 2015 [23].

Based upon PW Doppler examination alone, not all diastolic dysfunction grades of HFpEF are clearly distinguishable from the healthy heart. A comprehensive assessment of diastolic dysfunction through echocardiography should therefore integrate PW and tissue Doppler imaging [24]. However, the absence of elevated filling pressures during assessment at rest does not preclude patients from having profound haemodynamic impairments during exercise. HFpEF patients, especially at an early stage of the disease, are therefore easily missed. It has been proposed to introduce invasive stress testing for better identification means. Right heart catheterisation and cardiac magnetic resonance imaging are not standard procedure to date, but could improve diagnostic sensitivity and staging in HFpEF patients [25].

Cardiac tissue stiffness is at the heart of HFpEF

The heart of HFpEF patients demonstrates diastolic dysfunctional since the myocardial tissue becomes gradually stiffer, attenuating the relaxation of the LV during diastole [26]. Myocardial stiffness in HFpEF results of (1) qualitative and quantitative extracellular matrix (ECM) changes, such as increased deposition of interstitial collagen and more collagen crosslinking [27], and (2) stiffness of the cardiomyocytes themselves [28].

In the healthy heart, fibroblasts are responsible for the formation of the ECM by producing and secreting collagen. The cardiac ECM is mainly composed of thicker collagen type I fibres (~85%), which confer tensile strength, and thin collagen type III fibres (~11%), that maintain the elasticity of the matrix network [29]. In addition to collagens, the cardiac ECM also contains glycosaminoglycans (e.g., hyaluronan), glycoproteins (e.g., fibrillin), and proteoglycans (e.g., syndecan). Under pathophysiological stresses, such as aging, hypertension, T2DM, myocardial injury, toxic insults, and pressure overload, augmented cardiac fibrosis develops as a result of elevated levels of circulating transforming Growth Factor β (TGF-β). TGF-β

is a pro-fibrotic cytokine, present as a latent complex in the ECM of healthy hearts [30]. However, in HFpEF patients, circulating levels of TGF-β are elevated [31]. TGF-β mediates differentiation of fibroblasts into contractive and secretory myofibroblasts that contribute to cardiac fibrosis by promoting collagen deposition over degradation [32-33]. Collagenous septa detach and insulate cardiomyocytes, hampering myocyte-myocyte interactions ultimately contributing to cardiac dysfunction [32]. In addition to increased collagen depositions, collagen crosslinking raises through upregulation of the collagen crosslinker lysyl oxidase (LOX). Furthermore, increased LOX levels are associated with an impaired E/E' ratio in HFpEF patients [27].

Myocardial stiffness can be aggravated by intracellular cardiomyocyte alterations that stiffen the cardiomyocytes themselves. These changes occur due to modifications of the giant protein titin and reduced calcium (Ca^{2+}) signalling. Titin is a bidirectional spring in the cytoskeleton responsible for the distensibility of cardiomyocytes, which is defined as the end-diastolic pressure required to distend the LV to the end-diastolic volume [10]. HFpEF patients suffer from reduced distensibility indicated by an increased end-diastolic pressure [34]. Alternative splicing results in two titin isoforms: the longer, more flexible N2BA and shorter, but stiffer N2B isoform. Isoform switching from the more flexible N2BA to the stiff N2B increases cardiomyocyte stiffness and is observed in animal models of HFpEF and the associated comorbidities [35]. Besides isoform switching, the post-translational modification influences the cardiomyocyte stiffness. For example, hypophosphorylation of N2B at the protein kinase G (PKG) site also causes titin to become stiffer [36]. Secondly, cardiomyocyte relaxation depends on a drop of the cytosolic Ca^{2+} levels. Ca^{2+} is sequestered in the sarcoplasmic reticulum and extruded into the extracellular space upon activation of the cardiomyocyte [28]. Myocardial cytoplasmatic Ca^{2+} levels of HFpEF patients are elevated indicating impaired Ca^{2+} removal and thus impaired cardiomyocyte relaxation [37].

Excessive myocardial fibrosis, cardiomyocyte stiffness and attenuated active relaxation contribute to elevated LV diastolic stiffness, resulting in diastolic dysfunction in HFpEF patients [38-39]. During the early stages of the disease course, the relative importance of cardiomyocyte-based alterations of stiffness takes precedence over ECM-based changes, that become more prominent in the advanced stages [40]. Additionally, cardiomyocyte changes, such as elevated myofibrillar density and cardiomyocyte stiffness, induce cell growth in a transverse direction, while cell length is maintained constant. Consequently, cardiomyocyte concentric hypertrophy develops, as reflected by LV wall thickening and an increased wall-to-chamber radius ratio [41]. Furthermore, cardiomyocyte hypertrophy correlates with declined Protein Kinase G (PKG) activity in the HFpEF biopsies, which has been associated with decreased cardiomyocyte relaxation [42].

Cardiomyocyte relaxation is at least partly driven by the nitric oxide (NO) bioavailability in cardiomyocytes [43]. Paulus *et al*. proposed that a systemic inflammatory state was proposed to lowers NO bioavailability, which in the healthy heart is responsible for cardiomyocyte relaxation and inhibition of hypertrophic stimuli triggered by afterload excess (**Figure 4**). Cardiac nitrosative stress would thereby causes dysregulated NO-cGMP-PKG signalling, which induces three effects. Firstly, nitrosative stress inhibits the phosphorylation of phospholamban, which impairs active cardiomyocyte relaxation by reducing the phospholamban-mediated uptake of Ca^{2+} uptake in the sarcoplasmic reticulum. Secondly, hypophosphorylation of the N2B titin segment is hyperphosphorylated by low PKG activity, that elevates cardiomyocyte stiffness. Both the increased diastolic cytoplasmatic Ca^{2+} levels and cardiomyocyte

stiffness cause cardiac stiffening, resulting in attenuated LV filling [44]. Lastly, the decline in PKG activity allows for the development of cardiac hypertrophy as it cannot inhibit the hypertrophic pathways triggered by pressure overload anymore. Thus, the inhibition of PKG results in cardiomyocyte hypertrophy [45]. In HFpEF, LV hypertrophy occurs concentric which minimises cardiac wall stress as reflected by the normal circulating BNP concentration [9]. Additionally, systemic and microvascular inflammation would activate small numbers of invading inflammatory cells, expressing the pan-leukocyte marker CD45 [46–48]. Moreover, infiltrated leukocytes mediate TGF-β secretion, thereby promoting the differentiation of collagen-secreting myofibroblasts, which contribute to cardiac fibrosis [32], [33] (**Figure 4**).

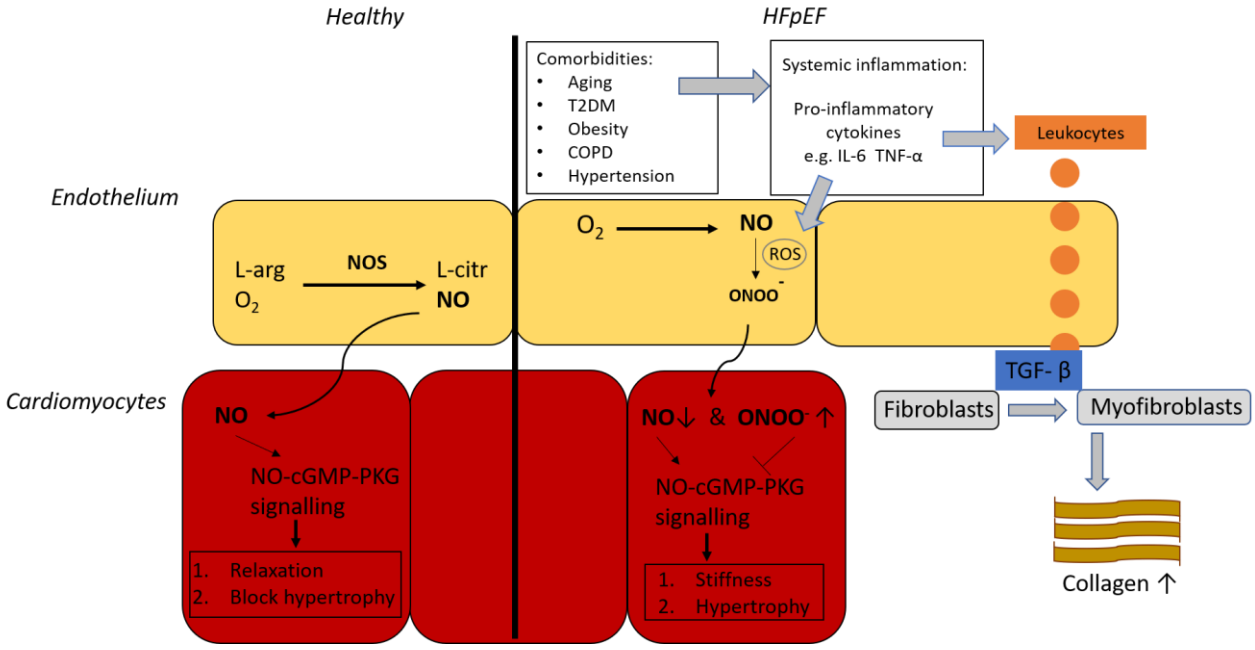

Figure 4. Nitrosative stress as a novel driver for HFpEF pathogenesis. Left. in the healthy heart L-arginine (L-arg) and oxygen are converted to L-citrulline and NO by NO Synthase. NO diffuses towards adjacent cardiomyocytes, where it activates cGMP-PKG signalling. PKG activity is responsible for cardiomyocyte relaxation and blocks different hypertrophic pathways. **Right**. The novel paradigm of Paulus *et al*. postulates that HFpEF-associated comorbidities such as aging, T2DM, Obesity, COPD, and hypertension induce a systemic inflammatory state. This state is reflected by a circulating profile of pro-inflammatory cytokines, like IL-6 and TNF-α. Resultant excessive ROS production on the one hand lowers NO bioavailability by converting NO to $ONOO^-$. On the other hand, promoted leukocyte infiltration causes increased levels of TGF-β, which stimulates the differentiation of fibroblasts into myofibroblasts leading to an excess deposition of collagen in the heart. The balance shift from NO to $ONOO^-$ in adjacent cardiomyocytes attenuates NO-cGMP-PKG signalling, which leads to cardiomyocyte stiffness and hypertrophy. O_2 = oxygen. NOS = Nitric oxide synthase. cGMP = cyclic guanosine monophosphate. PKG = Protein Kinase G. T2DM = Type 2 Diabetes Mellitus. COPD = Chronic Obstructive Pulmonary Disease. IL-6 = Interleukin-6. TNF-α = Tumour Necrosis Factor α. Peroxynitrite = $ONOO^-$. Reactive Oxygen Species = ROS. TGF-β = Transforming Growth Factor β. Adapted from Paulus, *et al*. 2013 [10].

3.2 Modelling HFpEF in the lab

A critical obstacle in the therapeutic innovation in HFpEF is the absence of animal models that accurately mimic the heterogenic complexity of human pathology. While the current evolving paradigm states that HFpEF development cannot be uncoupled from its comorbidities [10], the incomplete pathological understanding of HFPEF has hampered the development of novel therapeutics. Moreover, HFpEF patients are often oligo- or asymptomatic until late in the disease process, impeding standardised diagnosis upon

clinical signs and symptoms. HFpEF aetiology and pathophysiology are variable among patients [49], making HFpEF heterogeneous, encompassing a large spectrum of disease presentation and increasing the difficulty of clear diagnosis [50]. To improve the pathological understanding, the development of animal models mimicking human pathology is crucial. However, given the heterogeneity in exhibited comorbidities by patients, it is likely that any animal model only resembles a certain proportion of HFpEF cases. Relevant preclinical HFpEF models will be important to unravel the contribution of different comorbidities to the disease development and will provide mechanistic information. Moreover, existing animal models often result from complex breeding, which impairs genetic modification, further impeding the understanding of the underlying mechanisms in disease development [9].

An ideal preclinical model of HFpEF should meet three criteria. First, the induction of HFpEF in the animal model should reflect the known triggers in patients as closely as possible. As such, mild but chronic stimuli must be used, rather than stimuli with an acute onset. Second, the animals must mimic the human disease characteristics and symptoms as accurately as possible. This includes, measurable signs, such as an EF above 50% combined with diastolic dysfunction, exercise intolerance, pulmonary congestion, and myocardial remodelling [9]. Given the diseases heterogeneity, it is important that the set of comorbidities in the model are carefully selected for each research purpose. Lastly, the animal model should offer easy access to genetic manipulations in order to facilitate interventions as to elucidate key molecules and pathways in the disease progression. The more comorbidities involved, the more the animal model represents a complete HFpEF model, but this also complicates its genetic background countering easy genetic manipulation.

Zucker fatty and spontaneously hypertensive heart failure F1 hybrid (ZSF1) rat

The ZSF1 rat is developed by crossing rat strains with two different leptin receptor mutations (fa and fa^{cp}). A lean female Zucker diabetic fatty rat (+/fa) is crossed with a lean male Spontaneously Hypertensive HF rat (+/fa^{cp}) to generate both the obese and lean ZSF1 (fa/fa^{cp}) offspring. The obese ZSF1 rats are hypertensive and have unfunctional leptin receptors, leading to a disrupted energy balance. As a result, obese ZSF1 rats exhibit obesity, T2DM, and hypertension, resulting eventually in the development of HFpEF, while the lean heterozygous controls are only hypertensive [51]. The disease is presented by concentric cardiac LV hypertrophy, diastolic dysfunction with preserved EF, cardiomyocyte enlargement, cardiac fibrosis, and increased myocardial stiffness [52]. Furthermore, pulmonary congestion, impaired exercise tolerance, and chronic kidney disease are described [53-54]. The ZSF1 model is an acknowledged model for HFpEF, combining several comorbidities to mimic the human phenotype of different patient cohorts, however as it is a rat based model, genetic interventions to explore disease onset are largely unavailable [9].

db/db leptin receptor deficient mouse

The *db/db* mouse has a point mutation in the leptin receptor causing to hyperphagia, an extreme, unsatisfied drive to consume food, and spontaneous obesity accompanied by T2DM. The initial insulin resistance progresses towards deficient insulin secretion, similar to T2DM pathogenesis in humans [55]. Moreover, mice exhibit features of human T2DM, such as hyperglycaemia and increased circulating

glucagon levels, that are not present in weight-matched C57BL/6J mice fed a western diet [55]. Although *db/db* mice display diastolic dysfunction with preserved EF compared to *db/+* controls, they initially do not show cardiac hypertrophy and only develop it at older ages [56]. The animals show a systemic pro-inflammatory state in early disease (8 weeks), which dampens over time [57]. At the cellular level, elevated cardiac fibrosis, cardiomyocyte stiffness and capillary rarefaction are evidenced [58]. Pulmonary congestion paralleled by exercise intolerance and the reduced circulating BNP levels complete the required HFpEF phenotype [58-61]. Genetic interventions are possible in this model but are made difficult because they require time-consuming backcrossing of mouse colonies onto the *db/db* mutation. Additionally, both this model and the ZSF1 rats develop HFpEF due to a receptor mutation not common in human HFpEF development.

High Fat Diet and L-NAME fed mouse

Recently, Schiattarella *et al*. published a novel HFpEF model driven by concomitant metabolic and mechanical stress elicited by High Fat Diet (HFD) induces obesity and Nω-nitro-l-arginine methyl ester hydrochloride (L-NAME) induced hypertension, respectively [62]. In this model, C57BL/6N mice are subjected to a 5-weeks-long HFD and L-NAME treatment. L-NAME is a potent nitric oxide synthase (NOS) inhibitor that limits the NO bioavailability in endothelial cells (ECs) [63]. Since arteries normally dilate in response to acetylcholine through NO-cGMP-PKG signalling in relaxing smooth muscle cells, L-NAME administration functions as an endothelial dysfunction-based driver of hypertension [64-65]. Even, an inverse, contractile response to acetylcholine has been apparent when NOS was inhibited by L-NAME [66]. This 'two-hit' model displays worsened diastolic dysfunction with preserved EF, coupled to pulmonary congestion and exercise intolerance. At histological level, HFD + L-NAME treatment renders cardiomyocyte hypertrophy, cardiac fibrosis, and microvascular rarefaction [62]. The model used C57BL/6N mice, however, the vast majority of genetic models uses the C57BL/6J background, impairing their genetic modification. Both mice strains present with different physiological features. For example, the C57BL/6J has a higher systolic blood pressure, lower heart rate, and larger heart weight to tibia length compared to the C57BL/6N [67]. Furthermore, significant differences exist in immune response between both models [67]. Mating genetic models onto the 6J background is not feasible, since this requires 11 generations of backcrossing which would take approximately 2,5 years to achieve.

Spontaneous senescence prone (SAMP) mouse

The SAMP mouse is a model of accelerated senescence with a 40% shorter lifespan and rapid progression of age-related pathological phenotypes after maturation, such as neurodegeneration and carcinogenesis [68]. The most commonly used models in cardiovascular disease and cardiac aging are the SAMP8 mice [69]. SAMP8 mice develop diastolic dysfunction with preserved EF, which occurs independently of hypertension [68]. Cardiac remodelling is evidenced by increased LV stiffness, cardiomyocyte hypertrophy, elevated fibrosis, and moderate indications for cardiac hypertrophy in SAMP8 mice, compared to the senescence-resistant (SAMPR1) control mice [68]. Although this suggests the SAMP8 animals are suited to model diastolic dysfunction, the progress towards a full-fledged HFpEF disease state has not yet been described.

3.3 Microvascular regression as the driving mechanism for rarefaction

Next to functional cardiac aberrations and tissue remodelling, Mohammed *et al*. described an overall decline (~27%) in cardiac microvascular density (capillaries and arterioles) is described in HFpEF patients compared to age-matched controls [70]. Interestingly, this reduce in cardiac microvascular density positively correlated with cardiac remodelling in HFpEF patients [70]. A reduced density of the microvascular network in the vascular bed is referred to as microvascular rarefaction and signifies the imbalance between angiogenesis, the formation of new vessel from pre-existing vessels, and vessel regression, the ablation of selected branches [71]. However, the mechanism underpinning the reduced vessel density in HFpEF remains undefined.

Microvascular rarefaction was first described in the conjunctiva of hypertensive patients [72] but was also later shown to be the result of non-perfused vessels [73-74]. Microvascular rarefaction also occurs in other HFpEF-associated comorbidities, such as T2DM and hypertension. Decreased microvascular density impedes insulin and/or glucose delivery to muscles and adipose tissue, therefore driving the body towards systemic insulin resistance [75-76]. Therefore, the interest in capillary rarefaction in HFpEF patients is increasing. Moreover, according to preliminary data, a diabetic and hypertensive rat model for HFpEF exhibits coronary microvascular rarefaction at 21 weeks of age correlated with diastolic dysfunction (unpublished results, Cuijpers, *et al*.). In summary, coronary microvascular rarefaction occurs in comorbidities that precede established HFpEF and is therefore hypothesised to contribute to disease progression. The correlation between coronary microvascular rarefaction with cardiac remodelling in HFpEF further supports this concept [70].

The currents hypothesis for HFpEF disease progression lacks an explanation for coronary capillary rarefaction as observed in patients and the ZSF1 model [43]. New vascular beds in general are formed by producing an excess of blood vessels under pro-angiogenic conditions, while at later stages vascular remodelling will prune the vascular beds by capillary regression [71]. However, at the moment it is unclear whether cardiac rarefaction in patients' samples results from insufficient angiogenesis or excessive microvascular pruning [70]. Interestingly, preliminary results from our research group show that male ZSF1 rats display elevated vessel *regression* at 14 weeks, before the onset of HFpEF, and cardiac *rarefaction* at 21 weeks, with cardiac endothelial proliferation preserved at both time points of age (unpublished results Cuijpers, *et al*.). This suggests an active mechanism of vessel regression preceding HFpEF development. Moreover, endothelial dysfunction is linked with microvascular regression [71], effects of comorbidities, such as glycocalyx damage [77], disruption of interaction between endothelial cells in capillaries and their stabilizers, called pericytes, (unpublished data, Cuijpers, *et al*.) [71], and reduced blood flow and shear stress [78]. Taken together, microvascular rarefaction could alter the balance between molecular regulators of vessel maintenance and regression at the onset of HFpEF.

Regression can be assessed by the number of empty basement membrane sleeves per cardiac area normalised by the number of intact vessels. As the vascular endothelium matures, endothelial cells synthesize ECM proteins (e.g. collagen IV) to form a basement membrane supporting and enveloping endothelial cells and pericytes [79-80]. When the vessel regresses, endothelial cell apoptosis leaves an 'empty collagen sleeve' detectable for a short period, that serves as a historical record of pre-existing

vessels [81]. Afterwards, macrophages will degrade the collagen sleeve, leaving the regressed vessel undetectable (**Figure 5**). By co-staining endothelial cells and collagen (Col) IV, intact vessels can be distinguished by double staining for endothelial markers and col IV, while regressed vessels are only positive for Coll IV.

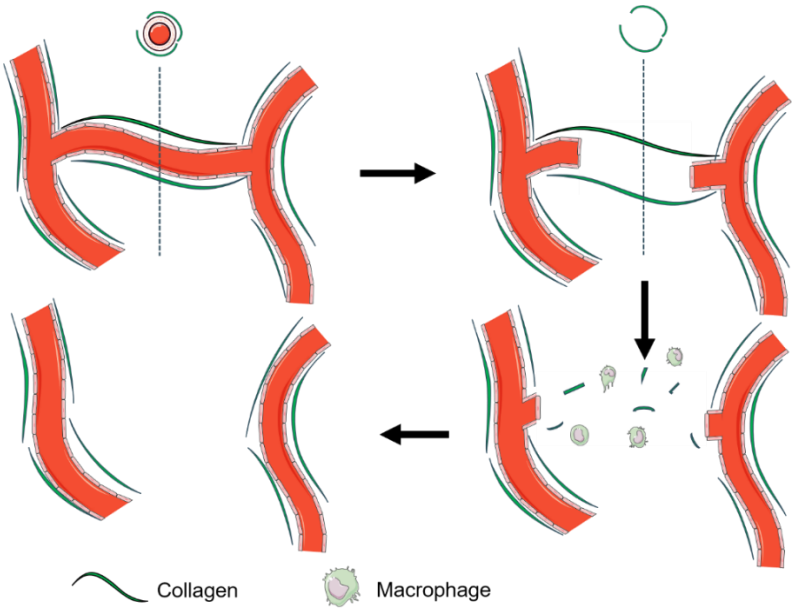

Figure 5. Sequential events in microvascular regression. Capillaries are surrounded and supported by a collagen IV. When the vessel is regressed an 'empty collagen sleeve' remains visible for a short period. Afterwards, macrophages degrade the collagen sleeve leaving the regressed vessel undetectable (unpublished data, Simmonds et. al).

Diminished microvascular density is associated with age-dependent decline of several pro-angiogenic factors, such as (endothelial) growth factors and enzymes of endothelial cell metabolism. For example, reduced levels of plasma insulin-like growth factor 1 (IGF-1) in elderly may induce vascular rarefaction in the brain, particularly since IGF-1 influences many aspects of blood vessel formation and repair [82]. Similarly, blocking signalling of all Vascular Endothelial Growth Factor (VEGF) isoforms in mice subjected to pressure overload promotes the progression towards heart failure. However, a diminished blood flow has been shown to induce capillary regression even in the presence of high levels of VEGF [83]. Another pro-angiogenic factor, called neuregulin 1 (NRG-1) attenuates endothelial senescence in the aorta and cardiac dysfunction in several HF animal models [84]. Sirtuin 3 (SIRT3), an NAD^+-dependent histone deacetylase, is known for its critical role in the regulation of endothelial glycolytic metabolism. Moreover, its expression reduces with age, suggesting a role in HFpEF disease progression. Disruption of SIRT3-mediated endothelial cell metabolism and impairment of endothelial cell-pericyte-cardiomyocyte communications may lead to coronary microvascular rarefaction and promote cardiac hypoxia, fibrosis and titin-modified stiffness, leading to HFpEF development [85-86].

Loss of endothelial Pitx2 expression coincides microvascular regression in the ZSF1 rat

Paired-like homeodomain transcription factor 2 (Pitx2) is mainly known for its role in left-right symmetry breaking of the developing embryo, which determines the further development of several organs, including the heart, lung and gut [87-88] (**Figure 6**). The *Pitx2* gene is discovered through its mutations

associated with the Axenfeld-Rieger syndrome [89-91], a syndromatic condition coursing with cardiovascular outflow tract malformations, eye dysmorphogenesis, craniofacial, and pituitary abnormalities [87]. *Pitx2* loss-of-function mice display early embryonic lethality associated with severe cardiac malformations [92], demonstrating the importance of Pitx2 during cardiogenesis. During midgut rotation, Pitx2, expressed exclusively on the left side of the embryo, is required for asymmetrical vessel development [93]. Additionally, maintenance of proper left Pitx2 functioning requires the presence of hyaluronan, a major component of the ECM that is stabilised upon heavy chain modification by tumour necrosis factor α-stimulated gene 6 (TSG-6). Whereas hyaluronan is bilaterally synthesised in the dorsal mesentery, only the right side is stabilised by TSG-6. Both correct expression of Pitx2 and TSG-6 are indispensable for the asymmetric vascular development in the gut [93] (**Figure 6**).

Pitx2 is increasingly being linked to programmed vessel regression. Downregulation of Pitx2 induced programmed microvascular regression in the primordial gut [94] and the developing aortic arch [95-96]. In ZSF1 rats this Pitx2 expression was reduced at 21 weeks as assessed by an RNAseq analysis (unpublished results of Heymans *et al.*). Furthermore, obese ZSF1 rats showed reduced Pitx2 expression in the endothelial cells at 14 weeks of age, which coincided with vessel regression in this model and preceded rarefaction (unpublished results, Cuijpers, *et al.*). This highlights the potential involvement of Pitx2 in vessel regression and suggests that rarefaction in HFpEF is being actively driven by an endothelial-specific loss of Pitx2 before disease onset.

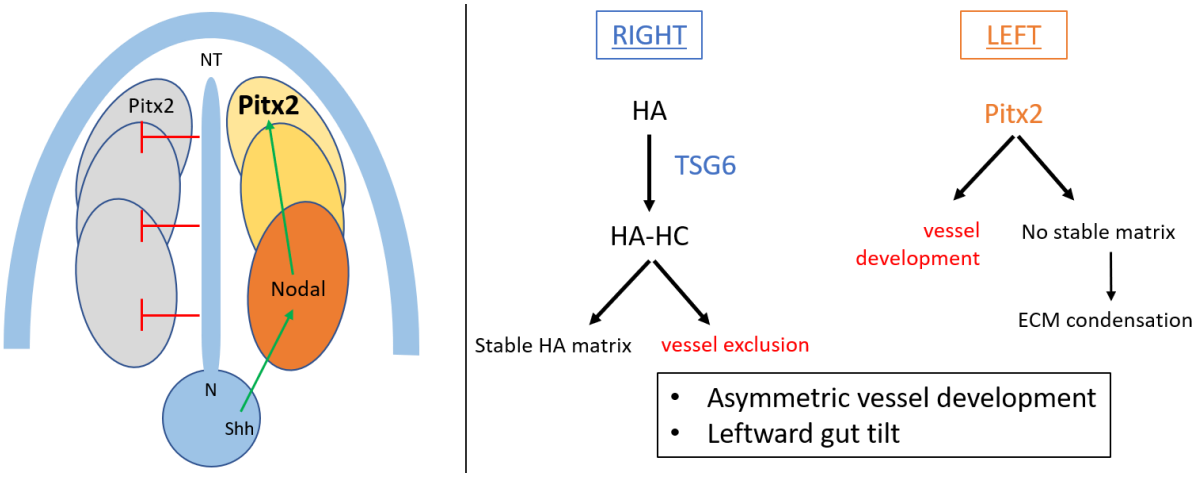

Figure 6. Left. The role of Pitx2 expression in left-right symmetry breaking during embryogenesis in mice. Left. From the node, Sonic hedgehog and Nodal induce Pitx2 expression uniquely at the left side of lateral plate mesoderm, while it is inhibited at the right side from the neural tube. **Right.** Pitx2 expression on the left side of the lateral plate mesoderm promotes vessel development at that side, while inhibiting the condensation of the extracellular matrix. Hyaluronan is uniquely modified with heavy chains by the TSG-6 enzyme at the right side, where it stabilises the ECM and contributes to vessel exclusion. Together, Pitx2 and HA regulate asymmetric vessel development and leftward gut tilt during embryogenesis. HA = hyaluronan. N = node. Shh = Sonic hedgehog. NT = neural tube. ECM = extracellular matrix. HC = heavy chains. Adapted from Sivakumar, *et al*. 2013 [93] and Franco, *et al*. 2017 [87].

4 HYPOTHESIS, AIM & OBJECTIVES

We *propose* that the development of HFpEF involves coronary capillary rarefaction, which occurs by an active regression process, rather than a passive loss of microvascular density, and which is driven by endothelial specific loss of Pitx2 expression.

In order to answer this question, this project *aims* to develop pre-clinical mouse models of HFpEF, with the potential to genetically ablate endothelial *Pitx2*. The current widely accepted HFpEF model is the ZSF1 rat model, in which cells-specific genetic ablations are not feasible.

Therefore, the *objectives* of this thesis are:

1. To identify the most appropriate HFpEF mouse model by comparing one recently published model (HFD + L-NAME treated mice) and two novel models (aged and *db/db* salt treated mice) that have differing comorbidity profiles.

2. To demonstrate that the loss of endothelial Pitx2 expression causes coronary microvascular regression and rarefaction *in vivo,* using an endothelial-specific *Pitx2*^{ECKO} mouse.

5 MATERIALS & METHODS

5.1 Animal models

Experiments were performed according to the Belgian law on the care and use of experimental animals (283/2014) and approved by the Animal Care and Use Committee of the University of Leuven (Project 217/2017). The animals were kept in ventilated cages housed in a breeding room under conventional conditions in 12-hour day and night cycle environment at 22°C. Chow diet (Ssnif® R/M-H, Ssniff Spezialdiäten GmbH, Soest, Germany; 9 kJ% fat, 24 kJ% protein, 67kJ% carbohydrates; 3,225 kcal/kg) and fresh water were provided *ad libitum*.

Aged C57BL/6J model

Aged male and female 6-month old control and 21-month old mice on a C57BL/6J background received a standard chow diet until echocardiography was performed, on the day of sacrifice (**Figure 7**).

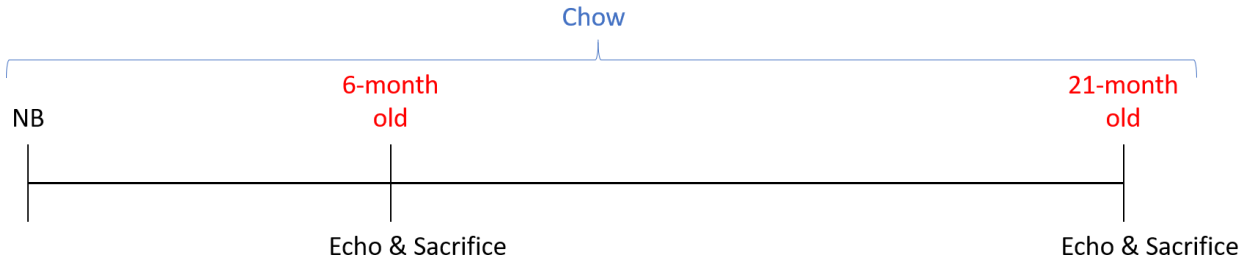

Figure 7. Aged C57BL/6J model experimental design. Newborn (NB) mice were raised on a chow diet and underwent echocardiography (Echo) just before sacrifice either at 6 months of age or at 21 months of age.

Salt treated db/db model

Male 6-weeks-old *db/+* or *db/db* animals for an OB-R leptin receptor mutation with a C57BLKS/J background were obtained from Jax (#000642). D*b/+* or *db/db* animals either received or did not receive an 8-week-long salt treatment in the water (10g/L), resulting in 4 experimental groups: (1) *db/+* without salt treatment (*db/+*), (2) *db/+* on NaCl treatment (*db/+* + S), (3) *db/db* without salt treatment (*db/db*), (4) *db/db* on salt treatment (*db/db* + S). Echocardiography (Echo) was performed at 14 weeks of age, 5 days before sacrifice (**Figure 8**).

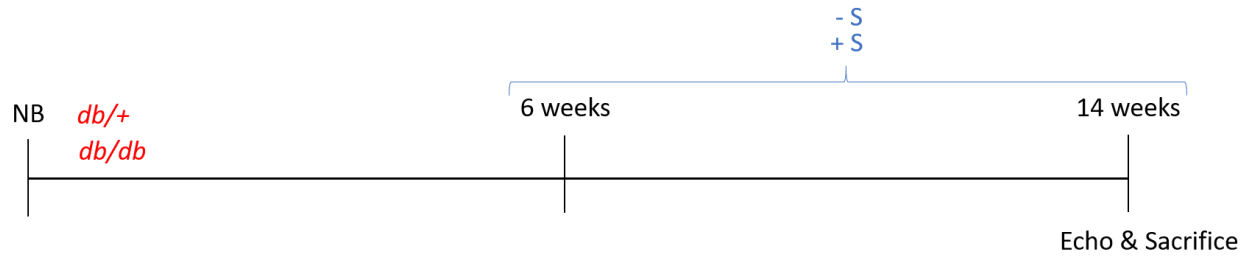

Figure 8. *db/db* salt treated model experimental design. Newborn (NB) heterozygous *db/+* and homozygous *db/db* mice were raised on a chow diet until 6 weeks of age, followed by either an 8-weeks-long salt treatment of 1% salt diluted in the drinking water (+ S) or control water without salt (- S), and echocardiography (Echo) at 14 weeks of age at 5 days before sacrifice.

High Fat Diet with L-NAME treated model

Male 9-weeks-old C57BL/6J wild-type animals received either (1) a chow diet, (2) a High Fat Diet (HFD; 60% fat, 20% proteins, 20% carbohydrates; D12492, Research Diet Inc., New Brunswich, NJ, USA) or (3) a two-hit combination of HFD with Nω-nitro-l-arginine methyl ester hydrochloride (L-NAME, 0.5 g/L; Cat. N. N5751, Sigma Aldrich, Overijse, Belgium) dissolved in the drinking water. Echocardiography was performed at 14 weeks of age, 5 days before sacrifice (**Figure 9**).

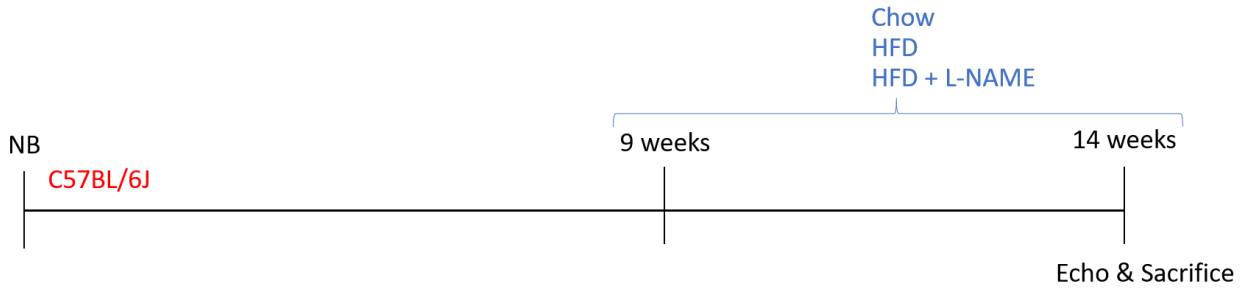

Figure 9. High Fat Diet + L-NAME model experimental design. Newborn (NB) C57BL/6J mice were raised on chow diet until 9 weeks of age, followed by a 5-weeks-long diet treatment of either control chow, High Fat Diet (HFD) or a combination of HFD and L-NAME dissolved in the drinking water, and echocardiography (Echo) at 14 weeks of age at 5 days before sacrifice.

Endothelial specific conditional Pitx2 knockout model (Pitx2^{ECKO})

To conditionally inactivate *Pitx2* in the endothelial cells of C57BL/6J animals (*Pitx2*^{ECKO}), males possessing the tamoxifen-inducible *Cre(ER)T2* recombinase gene controlled by an endothelial specific platelet derived growth factor (PDGF) promoter (*PDGF.iCre(ER)T2*$^{Tg/WT}$) and possessing a *Pitx2* gene where exon 4 is flanked by LoxP sites (*Pitx2*$^{fl/fl}$), were crossbred with females having only the *Pitx2*$^{fl/fl}$. The control group contained *Pitx2*$^{fl/fl}$ littermates that were negative for Cre(ER)T2 recombinase protein and the experimental group were the littermates that were *PDGF.iCre(ER)T2*$^{Tg/WT}$ *Pitx2*$^{fl/fl}$. Both control and experimental mice were injected with tamoxifen (0.2mg/g body weight) for three non-consecutive days (Monday-Thursday-Monday) at one week of age. Echocardiography was performed at 12 weeks of age (**Figure 10**).

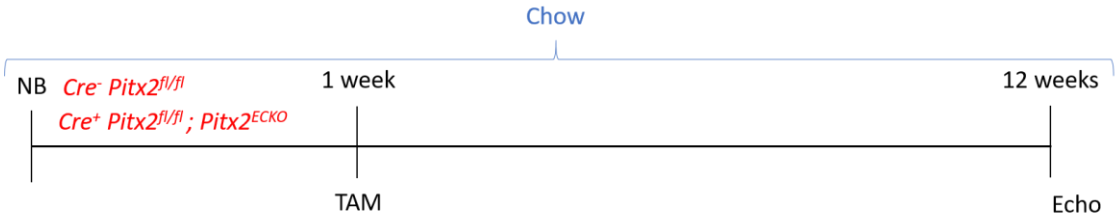

Figure 10. Pitx2$^{fl/fl}$ model experimental design. Newborn (NB) Cre recombinase negative *Pitx2*$^{fl/fl}$ control mice (*Cre*$^{-}$ *Pitx2*$^{fl/fl}$) and Cre recombinase positive *Pitx2*$^{fl/fl}$ mice (*Cre*$^{+}$ *Pitx2*$^{fl/fl}$*; Pitx2*^{ECKO}) were raised on chow diet and received 0.2mg/g body weight tamoxifen (TAM) injections at one week of age. Control chow diet was continued until echocardiography at 12 weeks of age.

5.2 Sampling

Echocardiography

Echocardiography was performed to assess cardiac haemodynamics, left ventricular dimensions, and systolic and diastolic functional parameters, two days before the sacrifice. Animals were anesthetised

with 5% inhaled isoflurane (Cuphar, Oostkamp, Belgium) for induction and 1.5% inhaled isoflurane for maintenance. Transthoracic 2-D M-mode and tissue and PW Doppler echocardiography was performed using a MS 400 transducer (18-38 MHz) connected to a Vevo 2100 echocardiograph (Visual Sonics, Toronto, Canada). Animals were placed in a supine position on a heating pad to maintain a body temperature, measured by a rectal probe, of 37.5-37.7 °C. The relevant clinical parameters were measured and calculated by a colleague skilled in echocardiography. Heart rate, LVIDd, and LVPWd were acquired on the parasternal short-axis transection using M-mode imaging and end-diastolic and end-systolic volumes were calculated according the Teichholz formula. Stroke volume and EF were calculated based on the M-mode images. LV blood filling was measured by PW Doppler trans-mitral flow tracings of E, A and DT, just above the tip of the mitral valve leaflets using an apical view. E' and A' were assessed with tissue Doppler imaging, at the lateral mitral annulus using an apical view. To evaluate diastolic function, E/E', E/A, E'/A' and A'/E' were calculated. At least three stable cardiac cycles were averaged for all measurements.

Tissue collection

Animals were weighed and were euthanized by an intraperitoneal injection of 100 mg/kg ketamine 100mg/kg (Nimatek, Eurovet, Bladel, The Netherlands) and 10mg/kg xylazine (Xyl-M®, V.M.D. nv/sa, Arendonk, Belgium) dissolved in 0.9% NaCl. Except from the aged mice and their controls, blood was collected and after making an incision in the right atrium, the LV was perfused with phosphate-buffered saline (PBS) to remove red blood cells form the tissue. Organs (heart, lungs, kidney, spleen, liver and brain) were collected, and the tibia length was measured to normalise the weights. Hearts of aged mice where perfusion-fixed using 4% paraformaldehyde (PFA). For every organ of the other models, one sample was stored at -80°C for future immunohistochemistry (IHC) and molecular biology techniques, such as western blot or RNAseq. A second sample was fixed in PFA, washed in ethanol and treated by a tissue processor (Leica TP1020 automatic tissue processor) for paraffin embedding and histological analysis.

5.3 Histology and Immunostaining

CD45 staining

To assess general inflammation, cardiac leukocyte infiltration was measured using an IHC staining for CD45, a pan-leukocyte marker. Paraffinized sections were dewaxed by xylol and rehydrated by ethanol and water in a series of 5-minute-long washing steps (two times xylol, two times 99% ethanol, 75% ethanol, 50% ethanol, distilled water). Sections were pre-treated with boiling citrate buffer (0.1M Target Retrieval Solution; DAKO S1699, Agilent, Santa Clara, USA) for 20 minutes for antigen retrieval and washed two times for 5 minutes with tris-buffered saline (TBS; 0.1M Tris-HCl pH 7.5 + 1.5M NaCl + 0.4% [v/v] Tween 20 [Cat. N. BP337500, Thermo Fisher, Waltham, USA] in distilled water). This was followed by treatment with a dilute hydrogen peroxide solution in methanol (1/100 H_2O_2 30% in MeOH) for 1 hour at room temperature (RT) to quench endogenous peroxidases and again followed by two 5-minute-long TBS washes. Slides were blocked in tris-NaCl-blocking buffer (TNB; 0.1M Tris-HCl pH 7.5 + 0.15M NaCl + 0.5% [w/v] TSA Blocking Reagent [Cat. N. FP1012; Perkin Elmer] in distilled water) for 45 minutes at RT, and washed two times for 5 minutes with TBS. Sections were then incubated overnight with rat anti-mouse

CD45 primary antibody (1/100 in TNB; Cat. N. 14-0451-82, Thermo Fisher, Waltham, USA) and three subsequent washes with tris-NaCl-tween buffer (TNT; 0.1M Tris-HCl pH 7.5 + 0.15M NaCl + 0,04% [v/v] Tween 20 in distilled water). Sections were stained for 1 hour long with goat anti-rat biotinylated secondary antibody (1/100 in TNB; Cat. N. 31830, Thermo Fisher, Waltham, USA) and 4',6-diamidino-2-fenylindool (DAPI; 1/1000 in TNB; Cat. N. D9542, Sigma Aldrich, Overijse, Belgium). After another series of three TNT washes, sections were incubated with a streptavidin-linked horseradish peroxidase (HRP) (1/100 in TNB; Cat. N. GERPN1231, Sigma Aldrich, Overijse, Belgium) for 30 minutes and followed by three 5-minute TNT washes. Freshly prepared tyramide working solution (Alexa Fluor 488 Tyramide SuperBoost™ Kit, Cat. N. B40922, Invitrogen, Carlsbad, USA) was added for 10 minutes at RT. Slides were washed three times for 5 minutes with TBS and mounted with ProLong™ Gold Antifade (Cat. N. P36930, Thermo Fisher, Waltham, USA).

Pictures of the stained sections were taken at a 40x objective magnification on an Axiovert 200M light microscope (Zeiss, Oberkochen, Germany). For every slide, 15 non-overlapping images of the left ventricle are obtained with a scale of 6.1996 pixel/µm. Cells that co-stained for CD45 and DAPI (CD45+/DAPI+) were considered as infiltrated leukocytes and blindly counted per cardiac area (µm²) using ImageJ software.

Sirius Red staining

To assess total (both interstitial and perivascular) fibrosis in the myocardium, the amount of fibrotic collagen tissue was measured using a chemical staining for collagen type I and III by Sirius Red solution (filtered 4% [w/v] picric acid [Cat. N. 197378, Sigma Aldrich, Overijse, Belgium] in distilled water + 0.1% [w/v] old red [Cat. N. 365548, Sigma Aldrich, Overijse, Belgium]). Paraffinized sections were dewaxed by xylol and rehydrated by ethanol and water in a series of 5-minute-long washing steps (two times xylol, two times 99% ethanol, 75% ethanol, 50% ethanol, distilled water). Sections were pre-treated with phosphomolybdic acid (0.2% in distilled water) for 5 minutes at RT before the 90-minute incubation of the tissue in filtered Sirius Red. The slides are washed in HCl (0.01M), dehydrated with a graded series of ethanol and xylol (45 seconds 70% ethanol, two times 3 minutes ethanol 100%, two times 3 minutes xylol) and mounted with Distrene Plasticizer Xylene (DPX; Cat. N. 06522, Sigma Aldrich, Overijse, Belgium).

Pictures of the stained sections were taken at a 40x objective magnification on an Axiovert 200M light microscope (Zeiss, Oberkochen, Germany). For every slide, 10 non-overlapping images of the LV were obtained. The percentage of collagen compared with the total amount of tissue within an image and excluding the lumen, as well as staining artefacts. Cardiac fibrosis was quantified, blinded for the origin of the samples, using ImageJ software.

Laminin staining and Collagen IV/DAPI co-staining

To determine cardiomyocyte hypertrophy, the cross-sectional area of cardiomyocytes was measured using an IHC staining for the laminin α chain as part of the basal membrane that outlines cardiomyocytes [97]. Pairs of paraffinized sections were dewaxed by as previously described. Sections were pre-treated with proteinase K epitope retrieval enzyme (1/500 in PBS; Cat. N. 21627, Sigma Aldrich, Overijse, Belgium) for 10 minutes, with a methanol (0.3% MeOH in H_2O_2) for 20 minutes and with 20% goat blocking serum

(Cat. N. ab7481, Abcam, Cambridge, UK) in TNB for 45 minutes at RT, each separated by 5-minute washes of PBS and TBS. Overnight incubation of the sections with rabbit anti-laminin α chain primary antibody (1/400 in TNB; Cat. N. L9393, Sigma-Aldrich, Overijse, Belgium) was performed. Three TNT washes were followed by a 45-minute-long incubation with goat anti-rabbit HRP-labelled secondary antibody (1/100 in TNB; Cat. N. P044801-2, Agilent, Santa Clara, USA). Sections were washed with TNT and twice with Tris-HCl. The sections were stained by applying a 3,3'-diaminobenzidine (DAB) containing solution (12,5% [w/v] DAB [SC-209686A, SC-biotechnology, Dallas, USA] + 0.325% H_2O_2 in Tris) for 2 minutes, washed three times for 3 minutes with distilled water, and counterstained with Harris Haematoxylin for 4 seconds.

In the *Pitx2*^{ECKO} model, cross-sectional cardiomyocyte area was assessed using a collagen (Col) IV/DAPI co-staining to visualise respectively the basal membrane and nucleus of the cardiomyocytes (see staining protocol below). Paraffinized sections were dewaxed and antigen retrieval was performed as previously described. Sections were blocked and incubated overnight with goat anti-mouse Col IV primary antibody (1/400 in TNB; Cat. N. 2150-1470, Bio-rad, Temse, Belgium) followed by 5 subsequent 10-minute-washes of TNT. A solution of donkey anti-goat AlexaFluor488-labelled secondary antibody (1/400 in TNB; Cat. N. A11055, Thermo Fisher, Waltham, USA) and DAPI (1/0000 in TNB) was applied for 1 hour.

Both laminin-stained and Col IV/DAPI-stained slides were washed under flowing tap water for 10 minutes, dehydrated with a graded series of ethanol and mounted with DPX.
Pictures of the stained sections are obtained at a 40x objective magnification on an Axiovert 200M light microscope (Zeiss, Oberkochen, Germany). For every slide 15 non-overlapping images of the left ventricle were collected. The cross-sectional area (µm²) of rounded non-elongated cardiomyocytes with a visible nucleus in the middle was quantified, blinded for the origin of the samples, using ImageJ software.

Collagen IV & Isolectin B_4 co-staining

To quantify the microvascular density and degree of vessel regression in the myocardium, an IHC co-staining was performed for Isolectin B_4 (IB_4) to visualise endothelial cells, together with Col IV to detect remnant empty collagen sleeves (Col IV^+ IB_4^-). Paraffinized sections were dewaxed and antigen retrieval was performed with citrate buffer as previously described. Sections were blocked for 30 minutes in phosphate-buffered saline with Triton (PBT; 0.1% Triton [Cat. N. T8787 Sigma Aldrich, Overijse, Belgium] in PBS), 30 minutes in TNB and three times 20 minutes in PBLec Buffer (1M $CaCl_2$ + 1M $MgCl_2$ + 0.1M $MnCl_2$ + 50% H_2O_2 + 1% Triton in PBS). Slides were incubated overnight with AlexaFluor488-labelled IB_4 (1/50 IB_4 [Cat. N. I21411 Thermo Fisher, Waltham, USA]) diluted in incubation buffer (0.5% Bovine Serum Albumin [w/v] [Cat. N. P6154, VWR, Oud-Heverlee, Belgium] + 0.25% Triton in PBS) and rabbit anti-mouse Col IV antibody (1/400 in TNB; Cat. N. 2150-1470, Bio-rad, Temse, Belgium), washed four times for 15 minutes with PBT, and incubated with donkey AlexaFluor568-labelled anti-rabbit antibody (1/400 in TNB; Cat. N. A10042, Life Technologies, Carlsbad, USA) for 1 hour. The sections were washed three times for five minutes in TNT and mounted with ProLong™ Gold Antifade.

Pictures of the stained sections were obtained at a 40x objective magnification on a confocal microscope. For every slide 10 non-overlapping images of the left ventricle, where the microvessels are cut cross-

sectionally, were collected. The number of intact vessels (Col IV^+/IB_4^+) and the regressed vessels (Col IV^+/IB_4^-) were counted, blinded for the origin of the samples, using Image J software, and used to calculate microvascular density and regression by the formulas below.

$$\text{Microvascular density} = \#IB_4^+ / \text{cardiac area}$$

$$\text{Microvascular regression} = \#\text{Col } IV^+ IB_4^- / \#IB_4^+$$

5.4 Statistical analysis

Data are shown as mean + SEM (standard error of the mean). Statistical analysis was performed using GraphPad software 7 (GraphPad Software Inc., La Jolia, California). Variance was tested with F-test ($p<0.05$) and normality was tested with Shapiro-Wilk test ($p<0.5$). Biological outliers were picked up based on Grubb's test ($p<0.05$). Normal data were analysed by an unpaired two-tailed t-test using GraphPad Prism. Non-normal data were analysed by a Mann-Whitney U t-test using GraphPad Prism 7. The data were considered as significant at $P<0.05$ (* $P<0.05$, ** $P<0.01$, ***$P<0.001$).

6 RESULTS

6.1 CHAPTER I: characterisation of HFpEF in 3 murine comorbidity models

HFpEF patients suffer from one or more comorbidities such as obesity, T2DM, hypertension, and aging, which are commonly considered as the drivers of HFpEF. The human variant of HFpEF involves an increased heart weight, pulmonary congestion, diastolic dysfunction and cardiac remodelling [62]. Therefore, an animal model for HFpEF must simulate (a combination of) these comorbidities and recapitulate the human phenotype. Moreover, to investigate the mechanics underpinning HFpEF pathophysiology, the animal model should be genetically modifiable. In this project, three different comorbidity mouse models were investigated: aged C57BL/6J animals*, db/db* mice given a 1% salt treatment for 8 weeks, and C57BL/6J mice given HFD + L-NAME for 5 weeks. The presence of HFpEF was examined in these models by looking at morphometric parameters, and cardiac function and remodelling.

Of all models tested, only 1% salt treatment in db/db mice induces obesity

To assess the obesity phenotype, and detect changes in heart weight and pulmonary congestion, all animals were morphometrically examined for total body and organ weight, which was normalised to tibia length.

Our 21-month old mice did not exhibit an obese phenotype, changed heart weight or pulmonary congestion. This was reflected by unaltered total body weight (**Figure 11A**), heart weight (**Figure 11D**), and lung weight (**Figure 11G**) normalised to tibia length compared to 6-month old controls. However, homozygous *db/db* leptin deficient mice given 1% salt treatment showed an increase in total body weight normalised to tibia length, indicating an obese phenotype compared to untreated *db/+* controls (**Figure 11B**). Despite this, the relative heart weight (**Figure 11E**) and lung weight (**Figure 11H**) remained unchanged. Surprisingly, the combinational treatment of a HFD and dissolved L-NAME did not elicit an obese phenotype compared to mice raised on a control chow diet (**Figure 11C**). Also, the heart (**Figure 11F**) and lung weight (**Figure 11I**) to tibia length ratio remained unchanged with respect to the control group.

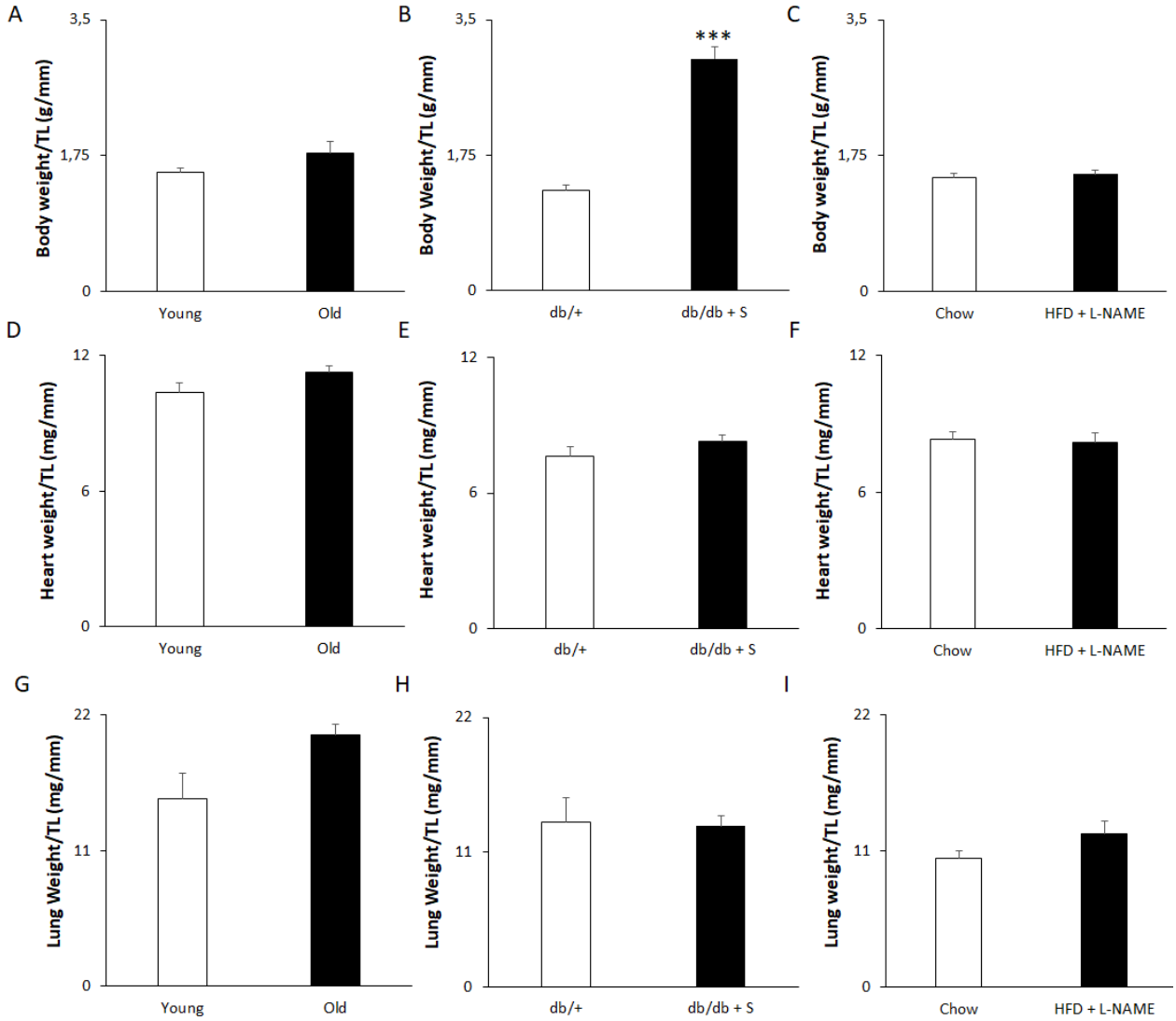

Figure 11. 1% salt treatment in db/db mice causes obesity. Aging and High Fat Diet with L-NAME treatment do not induce obesity. (A-C) Total body weight relative to tibia length in **(A)** Young and Old mice, **(B)** *db/+* control mice and salt treated *db/db* + S and, **(C)** chow fed mice and HFD + L-NAME treated mice. **(D-F)** Heart weight relative to tibia length in **(D)** Young and Old mice, **(E)** *db/+* control mice and *db/db* + S mice and, **(F)** chow fed versus HFD + L-NAME treated mice. **(G-I)** Lung weight relative to tibia length in **(G)** Young and Old mice, **(H)** *db/+* control mice and *db/db* + S mice and, **(I)** chow fed versus HFD + L-NAME treated mice. n = 8 for Young and Old, 9 for db/+, 8 for db/db + S, 5 for Chow and HFD + L-NAME. Data represented as mean + SEM. Statistical significance tested by an unpaired two-tailed t-test **(panels B-F, I)** or a Mann-Whitney test **(A, G, H)** depending on normality. *** p<0.001. TL = Tibia Length. Young = 6-month old mice. Old = 21-month old mice. db/+ = *db/+* control mice. db/db + S = 1% salt treated *db/db* mice.

All three models induced different stages of diastolic dysfunction

HFpEF patients exhibit diastolic function coupled to LV hypertrophy, while their systolic function is preserved. To assess the development of diastolic dysfunction in combination with a preserved systolic function in the three mouse models, M-Mode imaging and PW and tissue Doppler echocardiography were performed to assess parameters of systolic and diastolic function, as well as LV wall thickness.

The systolic function was unaffected in each model, as indicated by a preserved EF (**Figure 12A, B, C**) and stroke volume (**Table 1**). Aged mice showed no change in LV dimensions at diastole, including internal diameter (**Table 1**), posterior wall thickness (**Table 1**), and relative wall thickness (**Figure 12D**), visualised by M-mode imaging. Salt treated db/db mice however, showed an increased internal diameter (**Table 1**) compared to untreated db/+ controls. However, an unchanged posterior wall thickness (**Table 1**) and relative wall thickness (**Figure 12E**) do not support this observation. The internal diameter of HFD + L-NAME fed mice (**Table 1**) remained unaffected compared to the control mice, while the posterior (**Table 1**) and relative wall thickness (**Figure 12F**) were unexpectedly reduced.

PW Doppler echocardiography demonstrated that blood flow at the mitral valve remained unchanged between young and old animals, as shown by unaltered LV E and A peak velocity (**Table 1**), and DT (**Table 1**). Tissue Doppler imaging, revealed a reduced muscle relaxation capacity of the LV and thus stiffer cardiac tissue in old mice, as reflected by a decreased (less negative) E' (**Table 1**) although the A' peak of LV wall movement (**Table 1**), remained constant. This observation was supported by increased E/E' (**Figure 12G**) and E'/A' (**Table 1**) ratios, with no change in the E/A ratio (**Figure 12J**), indicating that aged mice represent with the pseudonormal stage of diastolic dysfunction.

PW Doppler in db/db + S mice indicated a more severe, restrictive stage of diastolic dysfunction. While A peak velocity (**Table 1**) and DT (**Table 1**) remained constant compared to db/+ controls, tissue Doppler imaging revealed a reduction in muscle relaxation capacity of the LV and stiffer cardiac tissue in db/db + S mice, as reflected by a lowered E' (**Table 1**). However, the A' peak of LV wall movement (**Table 1**), remained constant. This observation was supported by diastolic dysfunction criteria such as E/E' (**Figure 12H**) and E/A (**Figure 12K**), that were increased and decreased E'/A' ratio (**Table 1**) in salt treated db/db mice compared to control animals.

In HFD + L-NAME treated animals, the E peak of blood flow at early diastole (**Table 1**), the A peak velocity (**Table 1**) and the DT (**Table 1**) remained constant compared to controls. Tissue Doppler imaging demonstrated that E' and A' (**Table 1**) was unaltered. However, a reduction in muscle relaxation capacity of the LV was revealed by a decreased E'/A' ratio in HFD + L-NAME mice, compared to controls (**Table 1**). Although the E/E' ratio did not increase (**Figure 12I**, $p = 0.05563$), the elevated E/A ratio (**Figure 12L**) suggests a stage in between pseudonormal and restrictive diastolic dysfunction in HFD + L-NAME treated mice, compared to control animals.

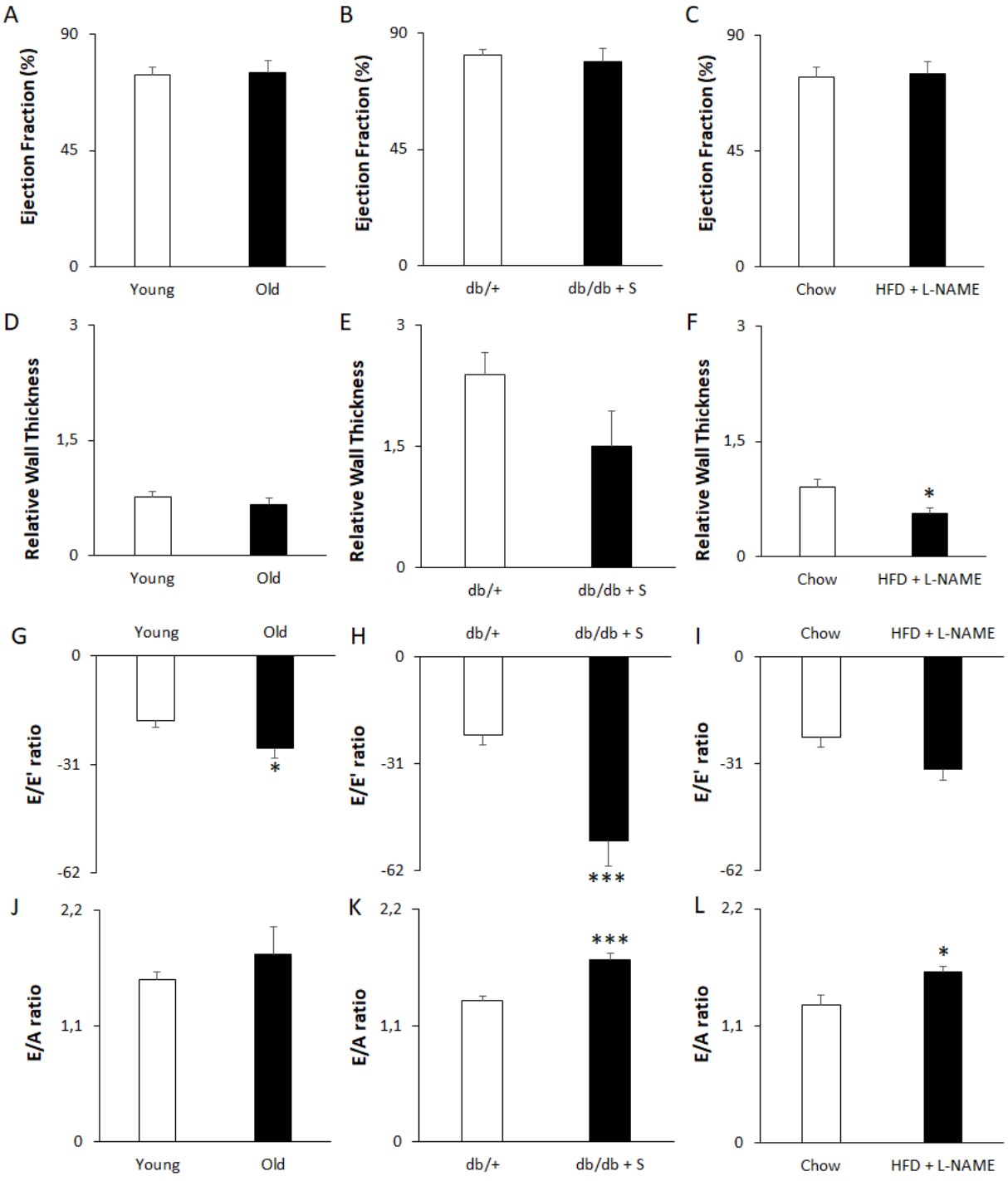

Figure 12. All three mouse models exhibit diastolic dysfunction with preserved EF. (A-C) Ejection Fraction measured in **(A)** in Young and Old mice, **(B)** *db/+* mice and *db/db* + S and, **(C)** chow fed and HFD + L-NAME treated mice. **(D-F)** Relative Wall Thickness in **(D)** in Young and Old mice, **(E)** *db/+* mice and *db/db* + S and, **(F)** chow fed and HFD + L-NAME treated mice. **(G-I)** E/E' ratio in **(G)** in Young and Old mice, **(H)** *db/+* mice and *db/db* + S and, **(I)** chow fed and HFD + L-NAME treated mice. **(J-L)** E/A ratio measured **(J)** in Young and Old mice, **(K)** *db/+* mice and *db/db* + S and, **(L)** chow fed and HFD + L-NAME treated mice. **A-F** assessed using M-Mode imaging. **G-I** assessed using PW and tissue Doppler imaging. **J-L** assessed using PW Doppler imaging. n = 8 for Young and Old, 9 for *db/+,* 7 for *db/db* + S, 5 for Chow and HFD + L-NAME. Data represented as mean + SEM. Statistical significance tested by an unpaired two-tailed t-test. * p<0.05, *** p<0.001. Young = 6-month old mice. Old = 21-month old mice. db/+ = *db/+* control mice. db/db + S = salt treated *db/db* mice.

Table 1. Echocardiographic parameters of the aged, *db/db* salt treated, and HFD + L-NAME animal model.

	Aged	*db/db* + S	HFD + L-NAME
Stroke volume (µl)			
LV Internal Diameter d (mm)		↑	
Posterior Wall Thickness d (mm)			↓
E peak velocity (mm/s)		↑	
A peak velocity (mm/s)			
Deceleration time (ms)			
E' peak velocity (mm/s)	↓	↑	
A' peak velocity (mm/s)			
E'/A' ratio	↓	↓	↓
Stage of diastolic dysfunction	**Impaired relaxation**	**Pseudonormal**	**Pre-restrictive**

Parameters were obtained by M-mode, PW Doppler, and tissue Doppler imaging. Statistical significance tested by an unpaired two-tailed t-test. ↑ $p<0.05$ increased. ↓ $p<0.05$ decreased. Empty cells represent unchanged parameters between experimental groups. LV = Left ventricle. d = at diastole. E = early mitral inflow blood peak velocity. A = late mitral inflow blood peak velocity. E' = early diastolic mitral annulus peak velocity. A' = late diastolic mitral annulus peak velocity.

HFD + L-NAME treatment causes elevated cardiac leukocyte infiltration

Next to functional cardiac aberrations, human HFpEF patients also suffer from cardiac remodeling accompanied by increased cardiac inflammation. We therefore stained heart sections to detect the leukocyte marker CD45 and assess leukocyte infiltration.

Both 21-month old mice and *db/db* mice treated with salt exhibited unchanged levels of leukocyte presences in the LV, compared to their respective controls (**Figure 13B, D**). HFD + L-NAME treated mice presented elevated levels of infiltrated leukocytes in the heart (**Figure 13F**). This was shown by an increased density of $CD45^+$ immune cells in the LV of HFD + L-NAME treated mice compared to control mice.

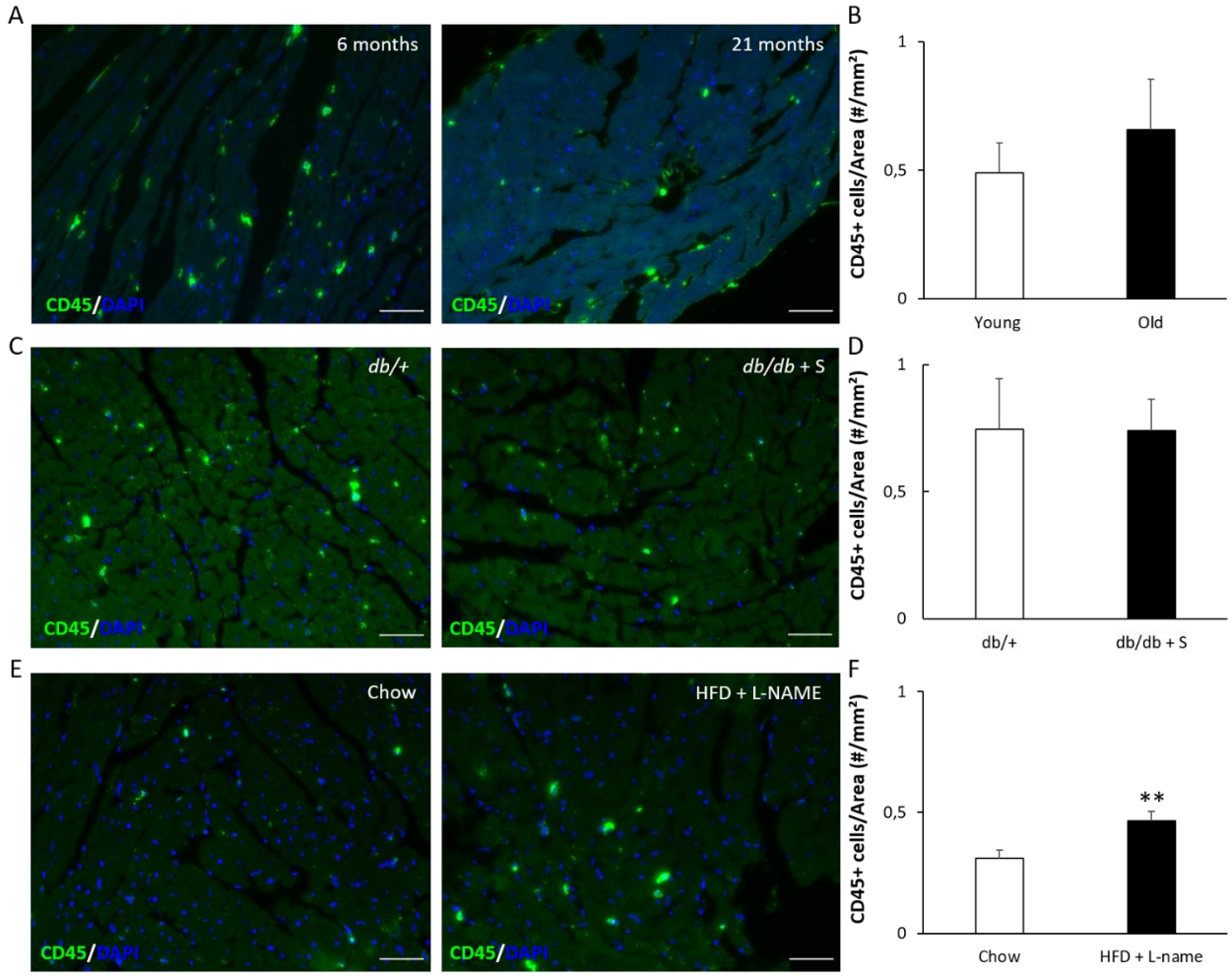

Figure 13. High Fat Diet + L-NAME treatment induces elevated levels of infiltrated cardiac leukocytes. (A, C, E) Representative images of CD45 staining in transversal heart sections from the LV of **(A)** Young and Old mice, **(C)** *db/+* mice and *db/db* + S and, **(E)** chow fed and HFD + L-NAME treated mice. **(B, D, F)** Density of $CD45^+$ cells per cardiac area quantified in **(B)** Young and Old mice, **(D)** *db/+* mice and *db/db* + S and, **(F)** chow fed and HFD + L-NAME treated mice. Scalebar = 25µm for all panels. n = 6 for Young, 7 for Old, 4 for *db/+,* 5 for *db/db* + S, 5 for Chow and HFD + L-NAME. Data represented as mean + SEM. Statistical significance tested by an unpaired two-tailed t-test. ** $p<0.01$. Young = 6-month old mice. Old = 21-month old mice. db/+ = *db/+* control mice. db/db + S = salt treated *db/db* mice.

Aging and HFD + L-NAME treatment cause cardiac fibrosis

Increased cardiac fibrosis is another hallmark of HFpEF. Total cardiac fibrosis was assessed by staining cardiac sections with Sirius red, which marks collagen in red collagen (**Figure 14**). Cardiac fibrosis was increased in both old animals and HFD + L-NAME treated mice compared to their respective controls (**Figure 14B, F**). Treatment with 1% salt did not affect the level of fibrosis in hearts of in *db/db* mice when compared to control (**Figure 14D**).

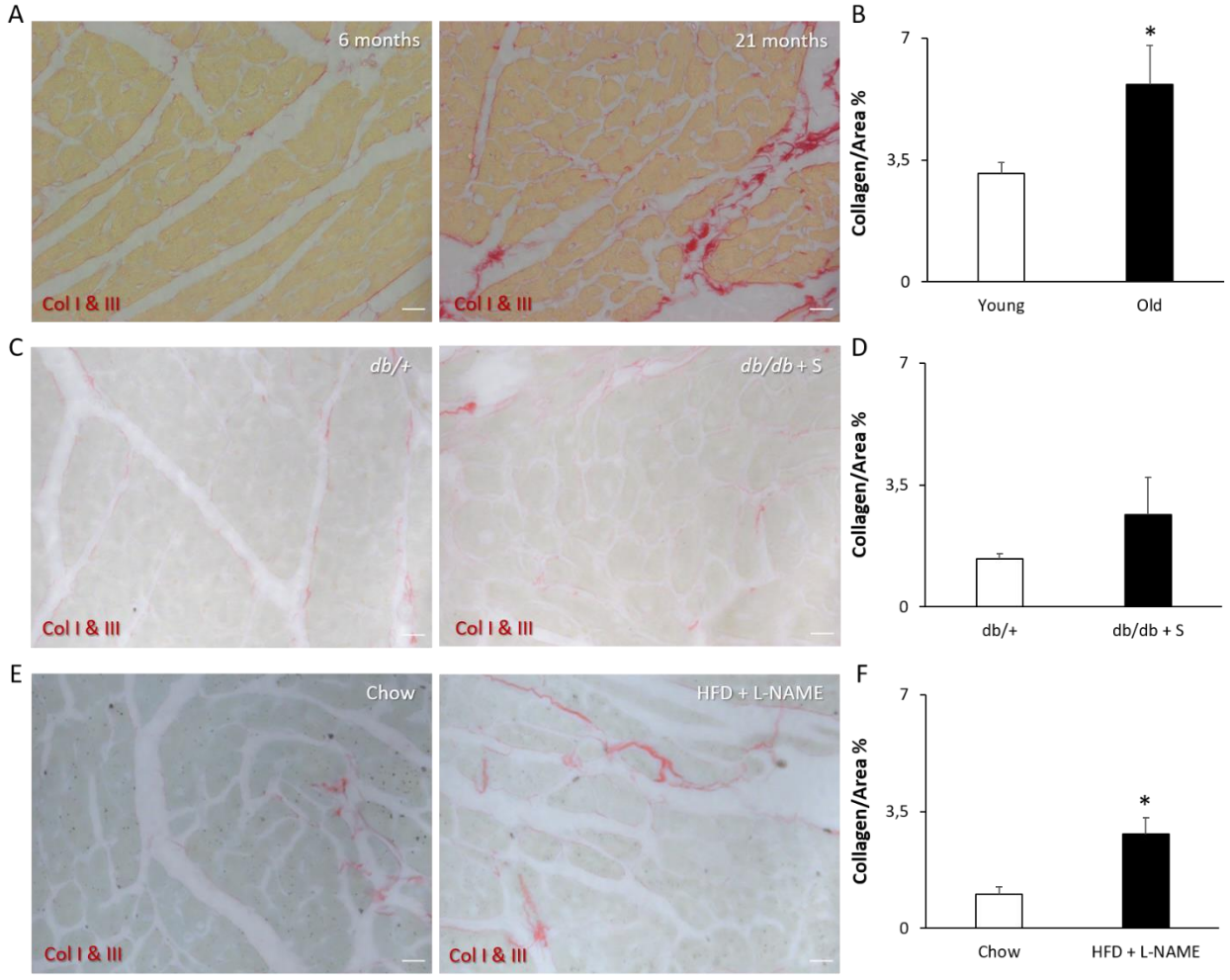

Figure 14. Age and High Fat Diet with L-NAME treatment induce increased cardiac fibrosis. (A, C, E) Representative images of collagen staining with Sirius Red in transversal heart sections from the LV of **(A)** Young and Old mice, **(C)** *db/+* mice and *db/db* + S and, **(E)** chow fed and HFD + L-NAME treated mice. **(B, D, F)** Percentage of collagen per cardiac area quantified in **(B)** Young and Old mice, **(D)** *db/+* mice and *db/db* + S and, **(F)** chow fed and HFD + L-NAME treated mice. n = 8 in Young, 7 in Old, 4 in *db/+*, 5 in *db/db* + S, 5 in Chow and HFD + L-NAME. Scalebar = 25 µm for all panels. Data represented as mean + SEM. Significance tested by an unpaired two-tailed t-test. * p<0.05. Col I & III = collagen I and III. Young = 6-month old mice. Old = 21-month old mice. db/+ = *db/+* control mice. db/db + S = salt treated *db/db* mice.

1% salt treatment in obese db/db mice induces cardiomyocyte hypertrophy

Cardiomyocyte enlargement, another feature of HFpEF, was assessed by laminin staining in all animal models (**Figure 15**). In both the aged and HFD + L-NAME model, cardiomyocyte size was comparable to their respective controls (**Figure 15B**). The *db/db* salt treated mice were the only to display cardiomyocyte enlargement, compared to control animals (**Figure 15D**).

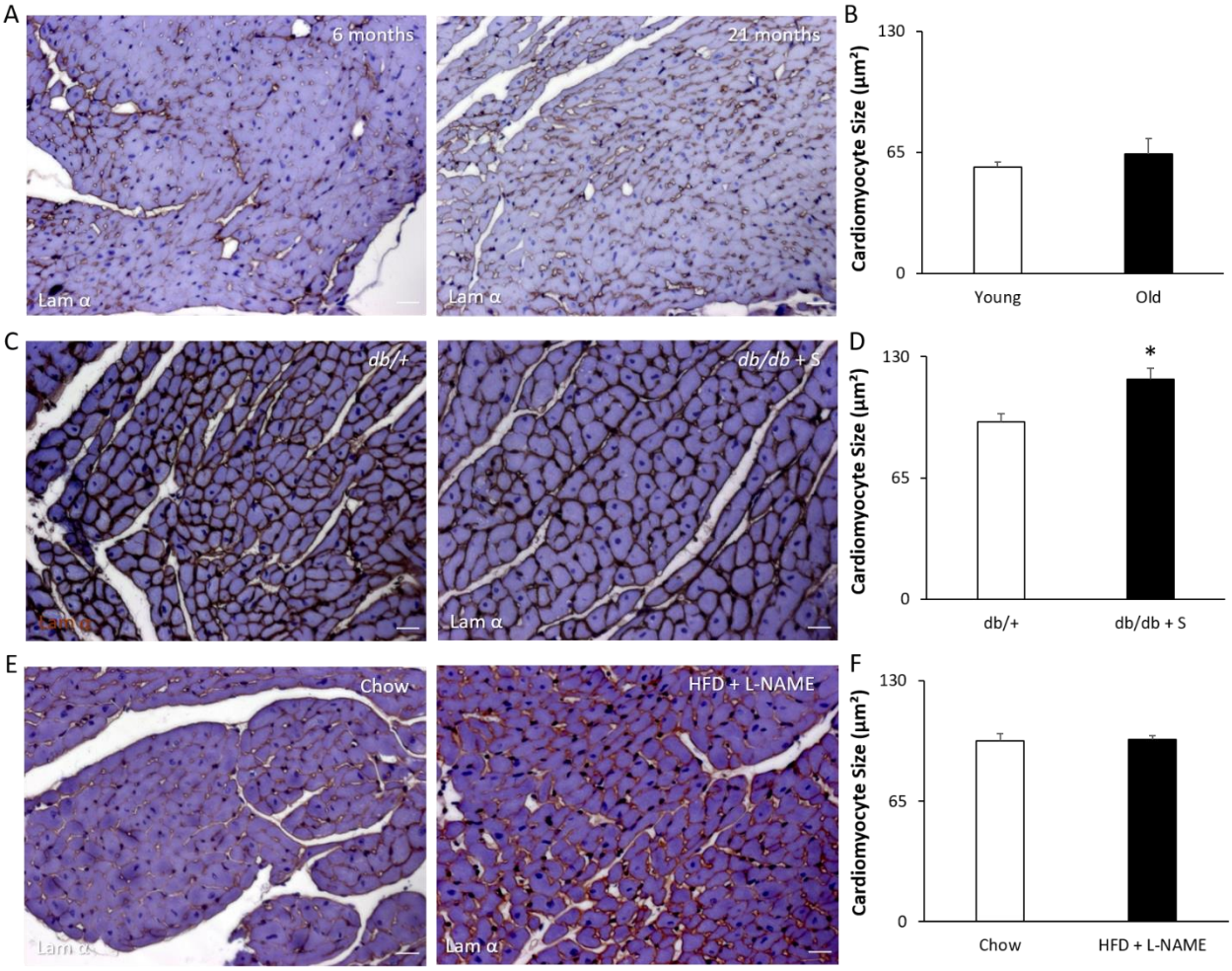

Figure 15. 1% salt treatment in obese db/db mice induces cardiomyocyte hypertrophy. **(A, C, E)** Representative images of laminin α (brown) IHC staining in transversal heart sections from the LV of **(A)** Young and Old mice, **(C)** *db/+* mice and *db/db* + S and, **(E)** chow fed and HFD + L-NAME treated mice. **(B, D, F)** Cardiomyocyte size quantified in **(B)** Young and Old mice, **(D)** *db/+* mice and *db/db* + S and, **(F)** chow fed and HFD + L-NAME treated mice. Scalebar = 25 µm for all panels. n = 8 in Young, 7 in Old, 3 in *db/+,* 7 in *db/db* + S, 4 in Chow, 5 in HFD + L-NAME. Data represented as mean + SEM. Significance tested by an unpaired two-tailed t-test. * p<0.05. Lam α = laminin α. Young = 6-month old mice. Old = 21-month old mice. db/+ = *db/+* control mice. db/db + S = salt treated *db/db* mice.

1% salt treatment in obese db/db mice causes coronary microvascular rarefaction

HFpEF patients exhibit as loss of cardiac vessels and cardiomyocyte hypertrophy is often accompanied by cardiac vessel density loss. IB_4 and Col IV co-staining by IHC was performed to investigate both vessel density and active regression. Rarefaction was measured as the density drop of intact $IB4^+$ vessels, and regression was calculated as the ratio of empty collagen IV sleeves to $IB4^+$ capillaries per cardiac area.

Old mice did not exhibit coronary microvascular rarefaction nor regression compared to young animals (**Figure 16B, C**). Interestingly, the salt treatment reduced microvascular density in the LV of *db/db* mice, as reflected by a reduced density of $IB4^+$ vessels per cardiac area, compared to the control group (**Figure 16E**). However, the ratio of empty collagen sleeves to $IB4^+$ vessels remained unchanged (**Figure 16F**). Finally,

cardiac microvascular density and empty collagen sleeves-to-IB4^{+} vessel ratio showed comparable rarefaction and regression between the HFD + L-NAME treated mice and controls (**Figure 16H, I**).

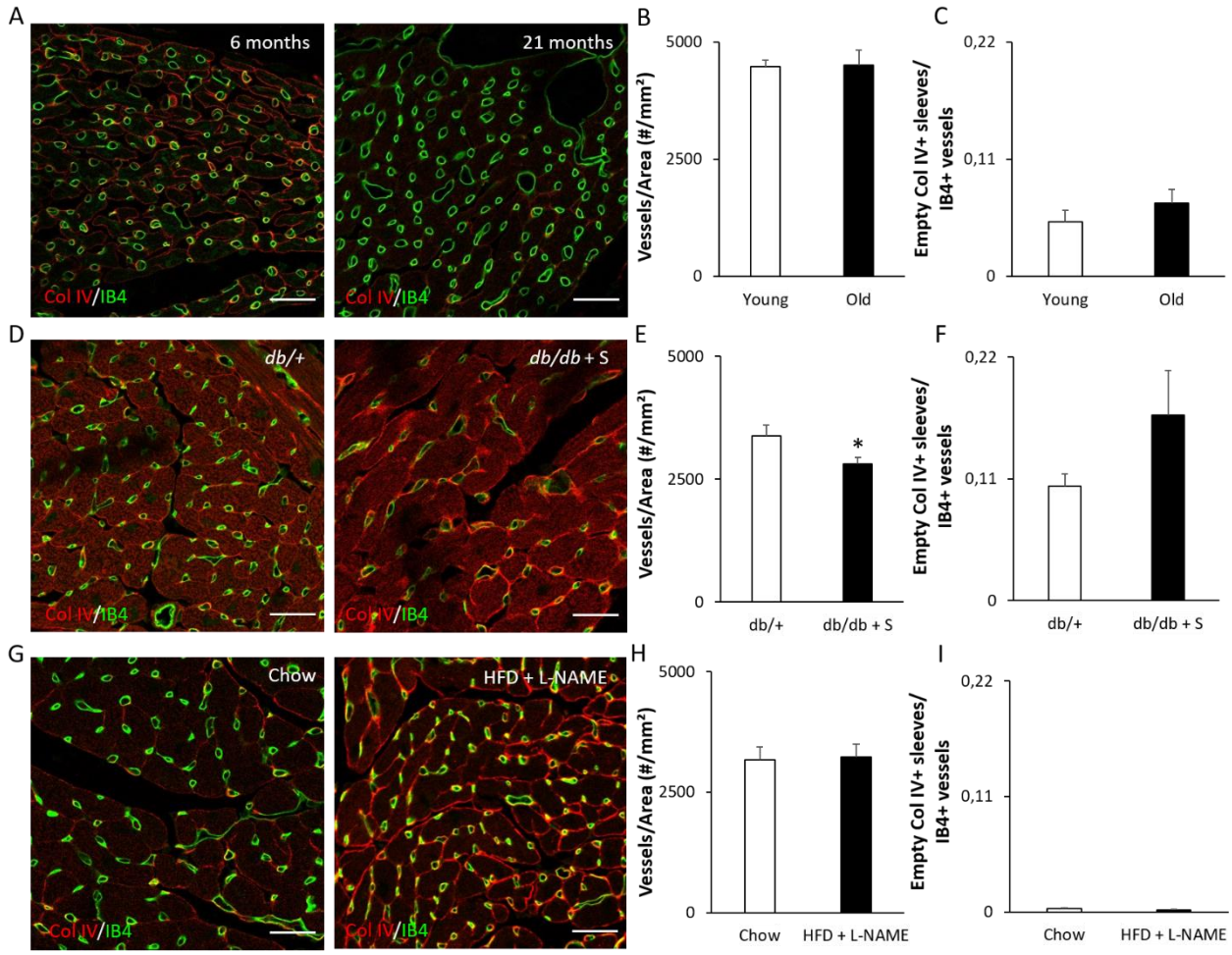

Figure 16. 1% salt treatment in obese *db/db* mice causes coronary capillary rarefaction. (A, D, G) Representative images of fluorescently labelled Col IV/IB_4 co-labelling in transversal heart sections from the LV of **(A)** Young and Old mice, **(D)** *db/+* mice and *db/db* + S and, **(G)** chow fed and HFD + L-NAME treated mice. **(B, E, H)** Rarefaction quantified as the density of IB_4+ vessels per cardiac area **(B)** Young and Old mice, **(E)** *db/+* mice and *db/db* + S and, **(H)** chow fed and HFD + L-NAME treated mice. **(C, F, I)** Regression quantified as the ratio of empty Col IV sleeves to IB_4+ capillaries per cardiac area **(C)** Young and Old mice, **(F)** *db/+* mice and *db/db* + S and, **(I)** chow fed and HFD + L-NAME treated mice. Scalebar = 25 µm for all panels. n = 8 in Young, 8 in Old, 5 in *db/+,* 6 in *db/db* + S, 3 in Chow, 5 in HFD + L-NAME**.** Data represented as mean + SEM. Significance tested by an unpaired two-tailed t-test. * p<0.05. Col IV/IB_4 = collagen IV/isolectin B_4. Young = 6-month old mice. Old = 21-month old mice. db/+ = *db/+* control mice. db/db + S = 1% salt treated *db/db* mice.

A summary of the results obtained in Chapter I is provided below (**Table 2**).

Table 2: Summary of functional changes and cardiac remodelling for all models tested.

	MV rarefaction	MV regression	Fibrosis	Cardiomyocyte enlargement	Leukocyte infiltration	DD stage	LV Hypertrophy (echo)
Aged			✓			Pseudonormal	
***db/db* salt treated**	✓			✓		Restrictive	✓
HFD + L-NAME (C57BL/6J)			✓		✓	Pre-restrictive	
ZSF1 rat (in preparation, Cuijpers, *et al.*)	21w	14w		✓	✓	DD	
HFD + L-NAME (C57BL/6N) (Schiattarella, *et al.*, 2019)	✓		✓	✓	Infl. mediator fingerprint	Restrictive	Heart weight/tibia length

MV = Microvascular. DD = Diastolic dysfunction. LV = Left ventricle. 21w = 21 weeks of age. 14w = 14 weeks of age. 'Infl.' = inflammatory. Schiattarella *et al.*, 2019 [62].

6.2 CHAPTER II: characterisation of the *Pitx2*^{ECKO} mouse

Pitx2 is known for its major role in cardiac development [87] and Pitx2 downregulation has been observed during programmed vessel regression in development [93]. Furthermore, we had previously found *Pitx2* downregulation in an RNA-Seq analysis of ZSF1 rat hearts (unpublished results, Heymans, *et al.*). To test whether Pitx2 plays a role in rarefaction during HFpEF development, a *Pitx2* endothelial deficient mouse model (*Pitx2*^{ECKO}) was created and investigated for HFpEF hallmarks. Endothelial *Pitx2* was deleted postnatally, to render the strongest possible phenotype. Adult ablation was combined with or without comorbidities induced by HFD + L-NAME and the presence of HFpEF was investigated. However, due to the Covid-19 pandemic, only the initial experiments are presented in this thesis.

Endothelial loss of Pitx2 at 1 week of age causes systolic dysfunction

Pitx2^{ECKO} mice displayed systolic rather than a diastolic dysfunction, in comparison to *Cre*$^{-}$ controls (**Figure 17**). Although the stroke volume remained unchanged (**Table 3**), there was a 20.7% decrease in EF (69.89%) (**Figure 17A**), as assessed with M-mode imaging. Both LV internal diameter (Table 3) and posterior wall thickness at diastole (**Table 3**) of *Pitx2*^{ECKO} mice were unaffected compared to control *Cre*$^{-}$ *Pitx2*$^{fl/fl}$ mice, resulting in unchanged relative wall thickness (**Figure 17B**). PW Doppler echocardiography indicated a lowered A peak (**Table 3**), while the E peak (**Table 3**), and the DT (**Table 3**) remained constant. Tissue Doppler imaging demonstrated an unchanged E' peak (**Table 3**) and the A' peak of LV wall movement (**Table 3**) in *Pitx2*^{ECKO} mice, compared to controls. Indicators of muscle relaxation capacity and diastolic dysfunction such as E/E' ratio (**Figure 17C**), E'/A' ratio (**Table 3**) and E/A ratio (**Figure 17D**) did not differ between experimental groups.

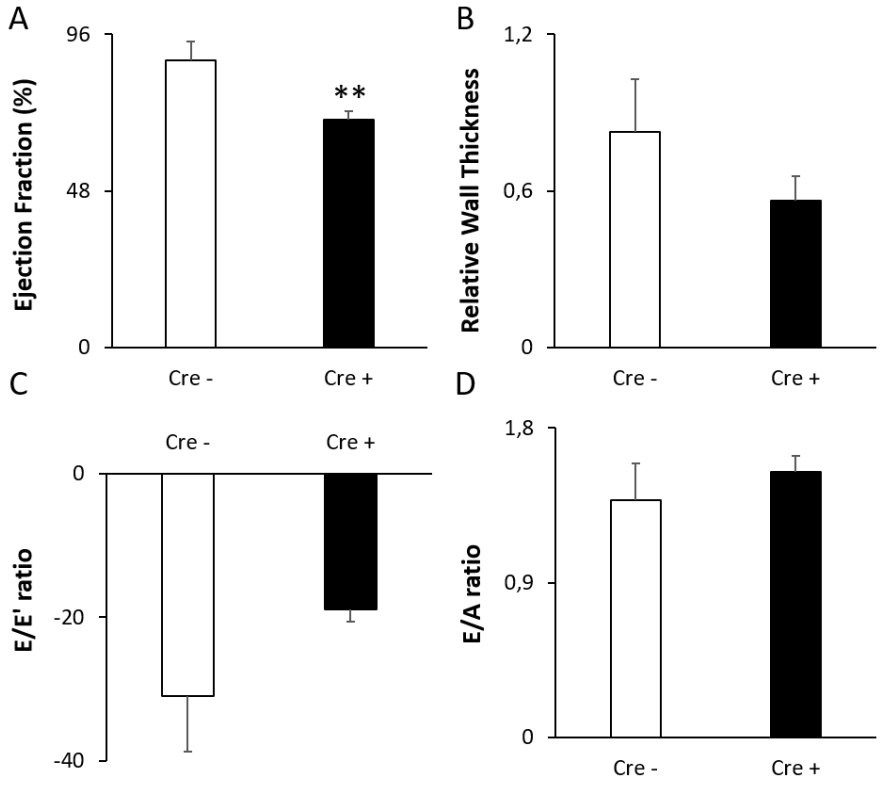

Figure 17. Endothelial-specific Pitx2 ablation causes systolic dysfunction. **(A)** Ejection Fraction assessed using M-mode imaging. **(B)** Relative wall thickness assessed using M-mode imaging. **(C)** E/E' ratio assessed by using both PW Doppler and Tissue Doppler imaging. **(D)** E/A ratio assessed by PW Doppler echocardiography. n = 6 for *Cre*$^{-}$ *Pitx2*$^{fl/fl}$, 4 for *Cre*$^{+}$ *Pitx2*$^{fl/fl}$ per group. Data represented as mean + SEM. Statistical significance tested by an unpaired two-tailed t-test. ** p<0.01. Cre + = *Cre*$^{+}$ *Pitx2*$^{fl/fl}$; *Pitx2*^{ECKO}. Cre - = *Cre*$^{-}$ *Pitx2*$^{fl/fl}$.

Table 3. Echocardiographic parameters of the *Pitx2*^{ECKO} mice.

	Cre^{+} *Pitx2*$^{fl/fl}$ vs *Cre*$^{-}$ *Pitx2*$^{fl/fl}$
Stroke Volume (µl)	
LV Internal Diameter d (mm)	
Posterior Wall Thickness d (mm)	
E peak velocity (mm/s)	
A peak velocity (mm/s)	↓
Deceleration Time (ms)	
E' peak velocity (mm/s)	
A' peak velocity (mm/s)	
E'/A' ratio	
Cardiac dysfunction	**Systolic dysfunction**

Parameters were obtained by M-mode, PW Doppler, and tissue Doppler imaging. Statistical significance tested by an unpaired two-tailed t-test. ↓ $p<0.05$. Empty cells represent unchanged parameters between experimental groups. LV = Left ventricle. d = at diastole. E = early mitral inflow blood peak velocity. A = late mitral inflow blood peak velocity. E' = early diastolic mitral annulus peak velocity. A' = late diastolic mitral annulus peak velocity.

Endothelial loss of Pitx2 at 1 week of age causes coronary microvascular rarefaction

Pitx2^{ECKO} mice present with a decreased coronary microvascular density (**Figure 18B**), without an increase in empty Col IV basement membrane sleeves that indicate the presence of active vessel regression (**Figure 18C**). Despite this, levels of cardiac fibrosis and cardiomyocyte hypertrophy were unchanged at 16 weeks of age compared to control animals (**Figure 18E,G**).

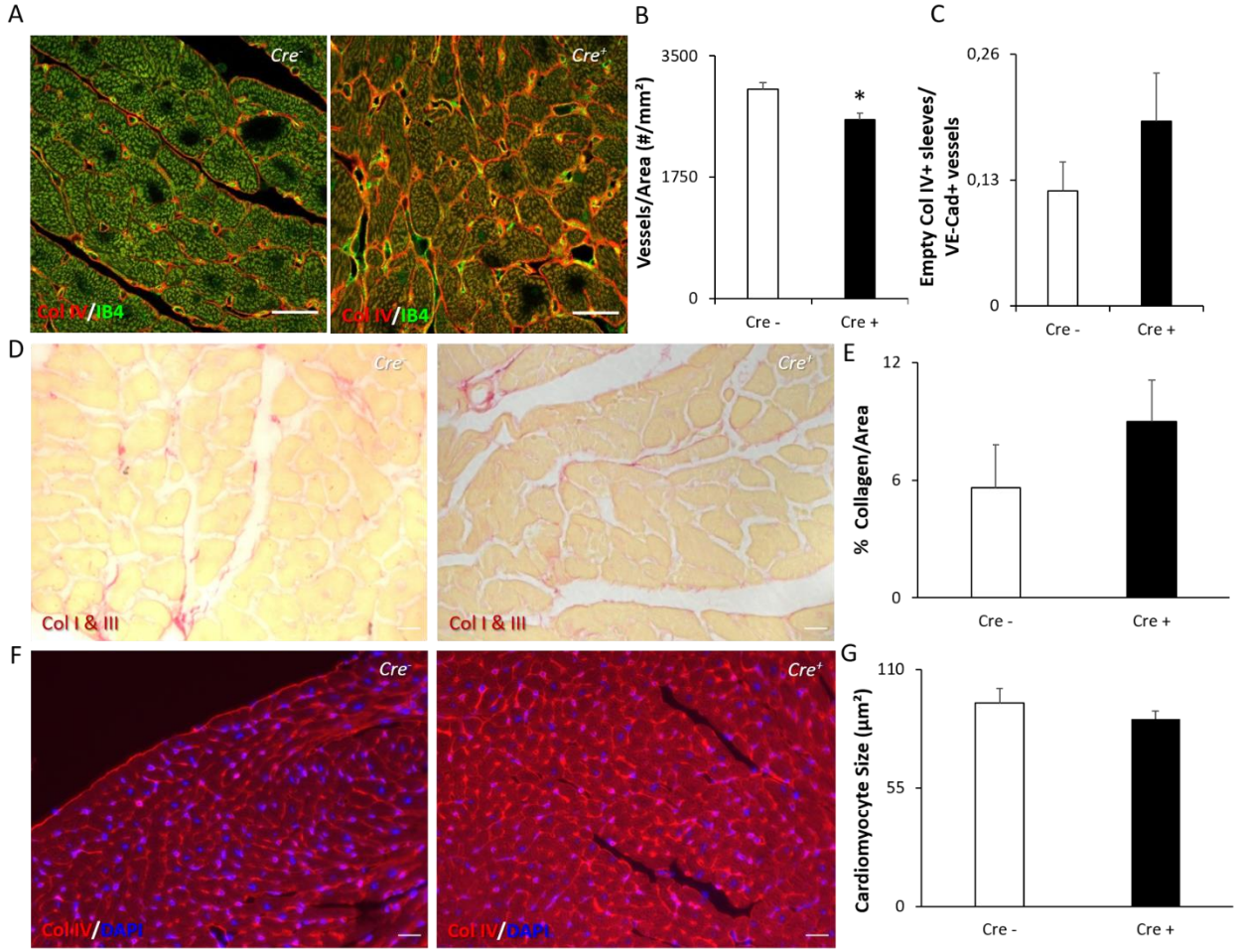

Figure 18. Endothelial-specific Pitx2 ablation induces coronary microvascular rarefaction. (A, D, F) Representative images of transversal heart sections from the LV of *Cre⁻ Pitx2$^{fl/fl}$* and *Cre⁺ Pitx2$^{fl/fl}$* mice injected with tamoxifen at 1 week of age **(A)** fluorescently co-labelled with Col IV/IB_4, **(D)** chemically stained for collagen with Sirius Red, **(F)** fluorescently co-labelled with Col IV/DAPI. **(B)** Rarefaction quantified as the density of IB_4^+ vessels per cardiac area. n = 6 in *Cre⁻*, 5 in *Cre⁺*. **(C)** Regression quantification by the ratio of empty Col IV sleeves to IB_4^+ capillaries per cardiac area. n = 6 in *Cre⁻*, 5 in *Cre⁺*. **(E)** Percentage of fibrotic collagen tissue per cardiac area. n = 6 in Cre⁻, 10 in Cre⁺. **(G)** Cardiomyocyte size. n = 6 in *Cre⁻*, 9 in *Cre⁺*. Scalebar = 25µm for all panels. Data represented as mean + SEM. Statistical significance tested by an unpaired two-tailed t-test. * p<0.05. Col IV/IB_4 = collagen IV/isolectin B_4. Cre + = *Cre⁺ Pitx2$^{fl/fl}$; Pitx2^{ECKO}*. Cre - = *Cre⁻ Pitx2$^{fl/fl}$*.

7 DISCUSSION

The first objective of this thesis project was to characterise the development of HFpEF in murine models that could be used in combination with genetic ablation. HFpEF development was characterised based on morphometric (organ weight), functional (echocardiography) and histological analysis (cardiomyocyte size, fibrosis, and vascular density). The models tested closely resemble the human disease phenotype and will enable genetic manipulation to investigate the molecular basis of HFpEF disease progression. The second aim of this project was to unravel the function of Pitx2, whose expression is known to be reduced during HFpEF (unpublished results of Heymans, *et al*.). To do this, we used an endothelial specific *Pitx2*^{ECKO} mouse and investigated body and organ weight, cardiac function and remodelling.

7.1 CHAPTER I: *db/db* salt treated mice most accurately recapitulate human HFpEF

The three animal models characterised in this project were based on two established models (aged mice and *db/db* mice) and one recently published mouse model (HFD + L-NAME treated mice). Other aging models, such as the Fisher 344 rat and SAMP8 mouse, have been used previously to model diastolic dysfunction [9]. However, chronic physiological aging is preferred over accelerated aging, as found in the SAMP8 mice, since it mimics the human situation better. The *db/db* leptin receptor deficient mice, which become spontaneously obese and develop severe hyperglycaemia secondary to T2DM [58][98], were given salt supplemented water to additionally raise blood pressure [99]. Therefore, this model was supposed to reflect patients with three common comorbidities, obesity, T2DM and hypertension. In the HFD + L-NAME model, mice were treated with HFD + L-NAME for 5 weeks.

In all cases, a genetic background of C57BL/6J was preferred. The db/db mice are not on C57BL/6J per se, but on a very closely related background (C57BLKS). The original model for the HFD+L-NAME had been done on a C57BL/6N background [62]. Our aim was not to repeat their published results, but to investigate whether the model also works on the 6J background. The preference for the 6J background in all cases was in anticipation of using the model for analysis of genetically modified mice, such as the *PDGF.iCre(ER)T2*$^{Tg/WT}$ animals, most of which are only available on the C57BL/6J background. Changing genetic backgrounds requires 11 generations of backcrossing, or about 2 ½ years. As such, this is not a feasible alternative.

None of the models present with pulmonary congestion

Despite pulmonary congestion being an important surrogate of HFpEF, lung weights were unaffected between the experimental groups of all models (**Figure 11**). However, lung congestion is demonstrated in the *db/db* leptin receptor deficient model [60] and in the original study on the HFD + L-NAME model by Schiattarella *et. al*. It is however plausible that the approach of measuring pulmonary congestion by lung weight is too rudimentary to detect changes. Alternatively, congestion can be evaluated upon open alveolar area in sections stained with Haematoxylin and Eosin, or upon the ratio between wet and dry lung weight.

Only salt treated db/db mice exhibit obesity

Though all three models had the potential to become obese, this was only observed in the *db/db* salt treated mice. In agreement with previous studies [100-102], aged mice did not display body or organ weight gain, compared to the young controls (**Figure 11A**). Other aspects of obesity could explain the aging cardiac phenotype. A lowered muscle/fat weight ratio could normalise an increase in total weight. Body weight increases until 18 months of age were previously evident in C57BL/6J mice, however, were followed by body weight loss accompanied by a drop in body fat and musculoskeletal tissue [103]. This suggests that the aging process itself, in the absence of obesity, was sufficient to induce the functional (pseudonormal diastolic dysfunction) and histological aberrations (increased cardiac fibrosis) observed later. Together, these data indicate that the observed restrictive diastolic dysfunction and histological changes, including hypertrophy and rarefaction, result from the obese phenotype, and, presumably, from T2DM and hypertension.

In contrast, *db/db* mice on a salt diet developed obesity (**Figure 11B**). In our study, the lung weights were unaffected between the experimental groups, despite lung congestion being demonstrated in the *db/db* leptin receptor deficient model [60]. It is however plausible that the approach of measuring pulmonary congestion by lung weight is too rudimentary to detect changes. Alternatively, congestion can be evaluated upon open alveolar area in sections stained with Haematoxylin and Eosin. Together, these data indicate that the observed restrictive diastolic dysfunction and histological changes, including hypertrophy and rarefaction, result from the obese phenotype, and, presumably, from T2DM and hypertension.

Surprisingly, mice given a HFD + L-NAME treatment did not increase in normalised body nor organ weight (**Figure 11C**). Schiattarella *et al*. previously demonstrated profound total body ($p = 5.57 \times 10^{-6}$) and lung ($p < 0.001$) weight gain after the HFD + L-NAME treatment, compared to control mice [62]. We did observe elevated fat size in the abdomen during dissection, although it was not measured.

Our observed absence of obesity may be due to the different genetic background. The two genetic sub-strains diverge in their whole-body calorimetry and body composition [104]. C57BL/6J mice are characterised by a lower fat mass and percent adiposity, a slightly lower food intake, and lower rate of body weight gain, in comparison with C57BL/6N mice over a 6-week HFD period [104]. Therefore, the 5-weeks-long HFD treatment may not be long enough to induce obesity in C57BL/6J mice.

Though we investigated which mice develop obesity, we did not test the presence of other comorbidities such as T2DM, hyperlipidaemia, or hypertension in any of the model. Obesity is the leading risk factor for type 2 diabetes [105]. The *db/db* mice are an established model of type 2 diabetes [55][98], and thus it is likely that the obese *db/db* salt treated mice developed T2DM. Glucose intolerance and hyperlipidaemia were also reported in C57BL/6N mice in response to the HFD treatment [62]. Glucose tolerance can be assessed by analysing fasting glucose levels or by performing an intraperitoneal glucose tolerance test. To account for hyperlipidaemia, plasma lipid levels can be measured from blood plasma using an HDL/LDL colorimetric assay kit. Alternatively, cardiac lipid levels can also be tested in sections. Cardiac lipid levels, neutral triglycerides and adipocytes specifically, can be visualised by an Oil Red O staining. Lastly, the presence of hypertension in the *db/db* + S animals is well outlined in the literature [99], and is also described in the HFD + L-NAME treated mice [62]. Measuring blood pressures can be done non-invasively

using an occlusion tail cuff. We did attempt blood pressure measurements, however, several mice died during the process, presumably due to stress during the habituation to the restrainer. Since stress increases blood pressure, these measurements were valueless and extra optimisation for the protocol is required. Also in the aged model, it would be preferable to test the presence of additional comorbidities developing during the aging process

All models present with different stages of diastolic dysfunction

Our results demonstrate that aging mice to 21 months is sufficient to induce a pseudonormal stage of diastolic dysfunction (**Figure 12**). A stiffer heart and, therefore, reduced muscle relaxation capacity of the LV in aged mice, were reflected by decreased movement of the LV wall (E'), increased E/E' and A'/E' ratios, and a decreased E'/A' ratio (**Figure 12**). While E' is already lowered during early stages of diastolic dysfunction, changes in E/E', E'/A' and A'/E' only occur from pseudonormal diastolic dysfunction onwards. The aged mice thus present with pseudonormal diastolic dysfunction, which is further confirmed by a pseudonormal ratio of early to late mitral filling velocity (E/A) [23] (**Figure 12J**). In accordance, 6-month old SAMP8 mice develop diastolic dysfunction [106], and aged female B6D2F1 hybrid wild-type mice show impaired relaxation at 30 months, compared to their respective controls [107]. Together, these findings imply that the aging process itself can push the heart towards diastolic dysfunction, even in the absence of other comorbidities that are commonly seen as drivers of the HFpEF pathophysiology.

The *db/db* + S group exhibited restrictive diastolic dysfunction, a further progressed diastolic dysfunction stage than in aged mice (**Figure 12**). *Db/db* + S mice present with a stiffened heart, indicated by a decreased E', decreased E'/A' ratio, and increased E'/E ratio (**Table 1** & **Figure 12**). Together, these findings suggest an increased early-to-late LV filling ratio (E/A) (**Table 1**), conclusive for restrictive diastolic dysfunction [23]. Previous studies revealed the prolonged relaxation of the LV in 7 weeks old *db/db* mice [108-109] that was accompanied by increased expression and less phosphorylation of the titin isoform N2B [52][58]. Titin is a spring protein within cardiomyocytes and different isoforms and phosphorylation of this protein affect elasticity of cardiomyocytes. Pseudonormal diastolic dysfunction was demonstrated in 6-month old *db/db* mice, compared to WT controls, but was absent in another group's results at 2 months [98][108]. By comparison with our results, this suggests that the salt treatment accelerated diastolic dysfunction development, making restrictive diastolic dysfunction already detectable at 14 weeks of age (3.5 months).

In our results, L-NAME + HFD only elicited a pre-restrictive stage of diastolic dysfunction (**Figure 12**). Prolonging L-NAME treatment could, however, resolve the lack of a full-fledged restrictive stage. HFD + L-NAME treated mice were characterised by a stiffened heart compared to controls, as reflected by a decreased E'/A' ratio (**Table 1**), while E/E' (**Figure 12I**) did not increase ($p = 0.0556$). This observation coincided with and increased early-to-late LV filling ratio (**Figure 12L**), implying a stage of diastolic dysfunction between pseudonormal and restrictive diastolic dysfunction [23]. In contrast, the use of obese C57BL/6N animals in the original study drove the heart into a more extreme, restrictive form of diastolic dysfunction [62]. As mentioned above, C57BL/6N mice have a higher rate of body weight gain than C57BL/6J mice. The lack of obesity in the C57BL/6J animals could be deemed responsible for the missing restrictive diastolic dysfunction after the HFD + L-NAME treatment, as assessed by Schiattarella *et*

al. [62]. This highlights the possibility that an extended HFD + L-NAME treatment could result in obesity and subsequent restrictive diastolic dysfunction.

Cardiac leukocyte infiltration and fibrosis are only coupled in the HFD + L-NAME model

Here, pseudonormal relaxation in aged mice was accompanied by elevated cardiac fibrosis (**Figure 14B**), but the levels of infiltrated leukocytes remained surprisingly stable (**Figure 13B**). This suggests an increase in circulating pro-inflammatory and -fibrotic mediators during aging, rather than increased infiltrated secretory leukocytes in the heart itself, as proposed by Paulus *et al.* [10].

In the salt treated *db/db* mice both cardiac leukocyte infiltration (**Figure 13D**) and fibrosis (**Figure 14D**) were unaltered. Lean controls do not show difference in fibrosis as compared to obese patients [110], and cardiac macrophage were previously reported to be normal in 19-month old *db/db* mice [111]. Cardiac fibrosis, however, has been often been reported to increase in *db/db* mice [98][108][112]. Differences in age could explain our different results. Furthermore, longer salt treatment could also render the myocardial tissue more fibrotic. The resulting cardiac fibrosis would then, in addition to hypertension, contribute to the development a more severe stage of diastolic dysfunction.

In the HFD + L-NAME model, was the only model where leukocyte infiltration and fibrosis corresponded (**Figure 13F** & **Figure 14F**). Schiattarella *et al*. used a cytokine/chemokine array to describe an inflammatory fingerprint of released circulating mediators, such as TNF-α and IL-6, in the treatment group [62]. In this thesis, however, $CD45^+$ leukocyte infiltration served as a proxy for cardiac inflammation. Both methods assess inflammatory status, but they highlight different aspects. As we stated for the aged model, pro-inflammatory mediators, such as TNF- and IL-6, are potentially produced by circulating inflammatory cells, rather than by locally recruited leukocytes. Therefore, the observed increase in cardiac $CD45^+$ leukocytes in hearts of HFD + L-NAME animals should be considered more as a side effect, rather than an etiologic factor of cardiac remodelling. However, increased numbers of heart infiltrated $CD45^+$ leukocytes are still able to accelerate the damage to the heart.

Cardiomyocyte hypertrophy and enlarged heart are not consistently present in the models

In this project, aging mice up to 21 months was insufficient to induce cardiomyocyte hypertrophy (**Figure 15**). In contrast, cardiomyocyte enlargement was previously described in 24-26-month old albino FVB mice [102] and in *in vitro* cardiomyocytes originating from the Wistar Kyoto rat [113]. It is possible that if the 6-month old animals were compared to 30-month old mice, the heart would be exposed long enough to aging and resulting cardiac stiffening to increase the end-diastolic pressure, and inducing adaptive hypertrophy [41][114]. The cardiomyocyte enlargement in aged FVB mice was not accompanied by changes in normalised heart weight [102]. This suggests the presence of cardiomyocyte apoptosis, or, more likely, decreased myocardial tissue density, since apoptosis is not evidenced in HFpEF cardiac hypertrophy [115].

Obese *db/db* given salt exhibited enlarged cardiomyocytes (**Figure 15D**), while no changed heart weight was found between treatment groups (**Figure 11E**). Therefore, similar as in the aged model, this cardiomyocyte enlargement is suggestive for a density drop of the myocardium, rather than causing

absolute weight gain of the hypertrophic heart. Inhibition of apoptotic and autophagic genes improved diastolic dysfunction even though this was not accompanied by deceased apoptosis or autophagy [116]. It would be worthwhile to verify the number of apoptotic cells in cardiac sections, by visualising them with a Click-iT TUNEL AlexaFluor assay [116]. Presumably, a longer lasting salt treatment and subsequent cardiac fibrosis would induce clear cardiac hypertrophy in *db/db* mice, as was detected with echocardiography.

Despite cardiac fibrosis in the HFD + L-NAME group, mice displayed unaltered cardiomyocyte size (**Figure 15F**) and heart weight (**Figure 11E**), compared to controls. This is all in contrast to the effect of HFD + L-NAME treatment in C57BL/6N mice of the original study [62]. This difference is probably due to the differing genetic background and associated lower rate of body weight gain in our model. However, it should be mentioned that Masson's trichome staining of connective tissue was used to quantify cardiomyocyte size in the previous study, compared to laminin staining used here [62].

Only salt treated db/db mice exhibit coronary capillary rarefaction and active regression

Aging failed to induce coronary capillary rarefaction, nor was there evidence of active regression (**Figure 16B, C**). Results in rarefaction with age are contrasting. Rarefaction was previously observed in the heart of 21-month old mice that were phenotypically selected for extended reproductive life, versus 2-month old controls [117]. However, another study using Fischer rats, showed rarefaction at 20 months, but not at 4, 12 and 29 months [118]. As such, the rarefaction could also be transient in our model. Alternatively, capillary density was never reduced in the aged animals, compared to young controls, implying that cardiac fibrosis uniquely is responsible for the pseudonormal diastolic dysfunction observed.

The salt-treated *db/db* mice demonstrated coronary microvascular rarefaction compared to *db/+* controls (**Figure 16E, F**). Reduced microvascular density has been previously reported in 11-week old [58] and 6-month old *db/db* males, compared to their controls [98]. Prolonged hyperglycaemia contributes to skeletal muscle dysfunction with changes in capillary density [119]. Moreover, obese patients display a lower coronary microvascular density, compared to non-obese patients [110]. However, active microvascular regression, was not present in our salt treated *db/db* mice. The presence of empty collagen sleeves is a transient event. The fact that vessel density was already reduced could indicate that active regression had already occurred by this stage. Alternative, reductions in vascular density in this model could simply be due to enlargement of cardiomyocytes.

The presence of microvascular rarefaction in HFD + L-NAME treated C57BL/6N mice shown by Schiattarella *et al*. could not be replicated in the C57BL/6J mice [62]. The milder pre-restrictive diastolic dysfunction in our model, compared to the C57BL/6N background, is presumably the result of cardiac fibrosis alone since rarefaction is not present (**Figure 16H, I**). The stage of diastolic dysfunction observed in both the aged and HFD + L-NAME models are less severe compared to the restrictive diastolic dysfunction in the *db/db* salt treated animals, that was accompanied by cardiac rarefaction. Therefore, obesity could be contributively cause coronary rarefaction and subsequently worsen the diastolic dysfunction even to restrictive diastolic dysfunction, highlighting the importance of combined comorbidities once more.

Db/db salt treated mice most accurately recapitulate HFpEF

Taken together the observed differences between the three mouse models show that different comorbidity profiles induce variable HF phenotypes. The accuracy in which models recapitulate the human situation correlates with the extent in which their comorbidities contribute to HFpEF development. Although the HFpEF disease presentation of the aged model appears to be the least advanced, it still recapitulated a mild form of diastolic dysfunction and cardiac fibrosis, highlighting that advanced age *per se* can induces some of the HFpEF characteristics. Interestingly, the addition of a salt treatment to the already established *db/db* model deteriorates diastolic dysfunction, making it a better HFpEF model. Salt-induced hypertension can therefore be seen as an important contributor to HFpEF progression. The HFD + L-NAME model in this project lacked an obese phenotype due to its deviating genetic background compared to the original study [62]. Hence, the presence of obesity next to hypertension is indispensable in the comorbidity profile of this model.

A homozygous point mutation in the leptin receptor is not prevalent among HFpEF patients. Moreover, in the *db/db* mice, obesity is induced through hyperphagia, which poorly mimics the human situation. Lastly, diabetes in this model involves uncontrolled hyperglycaemia, which does not mimic the clinical situation where patients follow symptom management [120]. HFD is therefore more physiologically relevant. With HFD, weight gain occurs through the consumption of a 60% lard fat diet, which is more analogous to the situation found in patients.

We also had 2 methods to induce hypertension between our models, either high salt or L-NAME in the drinking water. Hypertension induced by excessive dietary salt consumption provokes water retention, high blood flow, and adverse vascular resistances, and hypertension [121]. L-NAME, on the other hand, does not mimic the human disease development, since patients do not consume this chemical. Administration of L-NAME induces hypertension by inhibiting the acetylcholine-induced relaxation of arteries via endothelial dysfunction [64]. L-NAME also interferes with endothelial cell functioning in coronary capillaries adjacent to cardiomyocytes and therefore stimulates HFpEF pathogenesis via the proposed HFpEF paradigm reported by Paulus *et al*., 2013 [43]. A major drawback of both the salt and L-NAME exposed mice models involves that they do not reproduce the slow disease onset occurring in (future) HFpEF patients [50]. Our chronic aging model exhibits a more advanced stage of diastolic dysfunction than aged accelerated SAMP mice, hence represents the most physiological trigger of diastolic dysfunction.

All models involved have advantages and disadvantages, even if they recapitulate the syndrome relatively close, highlighting the complexity of modelling HFpEF in the lab. The lack of a perfect HFpEF animal models attenuates the understanding of its pathophysiology and the development of new therapies. The best approach, therefore, it to use multiple models and identify consistent behaviours present in all of them, regardless of differing stimuli that induce disease onset.

7.2 CHAPTER II: endothelial Pitx2 loss induces systolic dysfunction and coronary microvascular rarefaction uncoupled of cardiomyocyte enlargement

As mentioned before, preliminary results in the obese ZSF1 rat model revealed active capillary regression at 14 weeks of age, while rarefaction only occurred at 21 weeks, together with unaltered cardiac endothelial cell proliferation (unpublished results, Ilona Cuijpers *et al*.). The 21-week old obese rats also showed decreased *Pitx2* gene expression in the heart as assessed by RNAseq. Moreover, endothelial-cell specific Pitx2 protein levels were lower at 14 and 21 weeks of age (unpublished results, Steve Simmonds *et al*.). Loss of Pitx2 has previously been shown to trigger vessel regression in developmental models [94]. Together, these results indicate a possible role for Pitx2 in capillary regression at the onset of HFpEF development. To test this hypothesis, cardiac function (echocardiography) and remodelling (fibrosis, cardiomyocyte hypertrophy, capillary rarefaction, and capillary regression) were investigated in a model of endothelial specific ablation Pitx2 (*Pitx2*^{ECKO}).

Endothelial Pitx2 loss at 1 week of age causes systolic dysfunction

Echocardiography unexpectedly demonstrated a reduction in systolic function after loss of Pitx2 at 1 week of age, rather than diastolic dysfunction (**Figure 17**). This was shown by a reduction in EF and without any changes in diastolic function parameters. In human HF, a reduced EF value of 69,9 (+- 2,46 SEM)%, is still perceived as 'preserved', since only an EF lower than 40% is referred to as 'reduced EF' [7]. Moreover, the stroke volume remained constant, in contrast to reduced stroke volume in HFrEF patients. Thus, the observed phenotype was more in line with dilated cardiomyopathy [122].

The observed systolic dysfunction in this 1-week old *Pitx2*^{ECKO} mouse is potentially caused by loss of vascular density as the heart is growing. This will have different effects than rarefaction in a mature heart, where the cardiomyocytes are post-mitotic and terminally differentiated. During growth, a lack of vascular density could affect cardiomyocyte expansion, multi-nucleation and polyploidy [123], resulting in less cardiac muscle. In the mature heart, no new creation of mass is needed. To address this, the timing of tamoxifen injections in mice were changed to 7 weeks of age in a second ongoing experiment, to circumvent interference of heart growth with Pitx2 endothelial cell function.

Endothelial Pitx2 loss at 1 week of age induces coronary microvascular rarefaction uncoupled from cardiomyocyte enlargement

The endothelial specific loss of Pitx2 caused reduced capillary density (**Figure 17**), while cardiac fibrosis (**Figure 14**) and cardiomyocyte size (**Figure 15**) remained constant, compared to controls. Many believe that rarefaction occurs secondary to cardiomyocyte hypertrophy, as enlarging cells spread the microvessels out, resulting in a lower vessel density. However, recent evidence suggests it is an active process occurring before or simultaneously with cardiomyocyte hypertrophy [124]. Here, the coronary rarefaction in *Pitx2*^{ECKO} mice occurred in the absence of myocardial hypertrophy, suggesting that endothelial Pitx2 loss drives active microvascular regression uncoupled of cardiac hypertrophy. To be certain of this, however, we need a model without heart growth and thus need to repeat these experiments in the older mice.

The active vessel regression mechanism underlying the observed coronary rarefaction, was not detected (**Figure 18**). The regression assay detects former vessels by means of empty collagen sleeves, before their degradation by macrophages, leaving only a short timeframe in which a regressed vessel can be detected. As rarefaction and regression were only assessed 11 weeks after the induction of endothelial Pitx2 loss, it is likely that regression was missed due to the degradation of empty sleeves by macrophages, while the result of regression (i.e. capillary rarefaction) was visible. Capillary regression analysis at an earlier time point could provide more insight. All in all, the Pitx2 deficient model still requires additional experiments before we can assess the role of Pitx2 in HFpEF and in vascular regression. Furthermore, the triggers of this Pitx2 loss in the presence of comorbidities need to be investigated.

7.3 CHAPTER III: proposed mechanism and future perspectives

Aging as proposed backbone process for comorbidity-induced HFpEF pathogenesis

Based on the integration of results in this project with available literature, we propose that the aging process could serve as the backbone for HFpEF pathogenesis, accelerated by experimentally induced comorbidities (**Figure 19**). In contrast, the recent endothelial dysfunction paradigm for HFpEF pathogenesis clusters aging and all other HFpEF associated comorbidities, to induce the onset of the disease development in the same manner [43]. However, management of one comorbidity fails to improve disease outcome, suggesting that different comorbidities act on different levels of HFpEF disease development. For example, even in the absence of clinical hypertension, there is an increased prevalence of LV hypertrophy with age coupled to worsening diastolic dysfunction and preserved systolic function [125]. Additionally, for the cohort of HFpEF patients that have hypertension, lowering blood pressure pharmaceutically does not improve outcomes [126], even though the approach ameliorates echocardiographic parameters in patients with diastolic dysfunction alone [127-128]. Similarly, weight loss improves LV hypertrophy and diastolic function [129], yet this strategy has not been specifically studied in the HFpEF population [130]. Thus, targeting one specific comorbidity is not sufficient to address HFpEF. Lastly, aging itself is an additional major contributor to HFpEF and cardiovascular diseases in general [131] and it can therefore be proposed that the process of aging is accelerated by the aforementioned comorbidities.

Cardiac senescence is accelerated by obesity-induced diabetes and hypertension which often concur in HFpEF patients [132-133]. Therefore, functional and histological myocardial changes caused by these comorbidities can obscure signs of intrinsic cardiac aging [114]. Hypertensive patients between 40-50 years old display a similar left atrium size, compared normotensive but advanced aged controls [134]. Across all age-cohorts, parameters of LV hypertrophy and diastolic dysfunction deteriorate [134]. In addition, hypertension accelerates aging-related alterations of endothelial function [135]. In Zucker Diabetic Fat rats, an established rat model for diabetes, the number of senescent aortic endothelial cells increase a 6-fold at 22 weeks of age [132]. The murine counterpart, *db/db* mice, show elevated cardiac levels of senescence biomarkers after 15 weeks of salt treatment [133]. Together, these findings suggest an indisputable importance for aging, accelerated by several comorbidities.

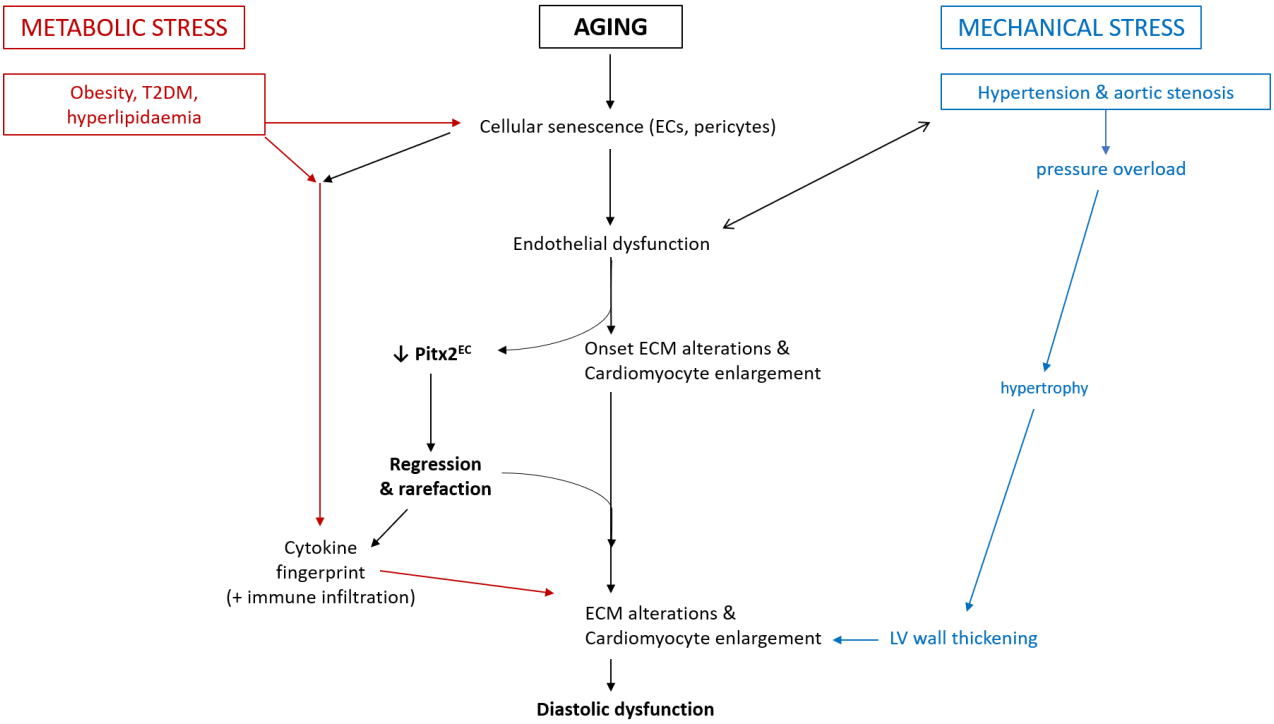

Figure 19. Aging as proposed backbone process for comorbidity-induced HFpEF pathophysiology. T2DM = Type 2 Diabetes Mellitus. ECs = Endothelial Cells. cGMP = cyclic Guanosine Monophosphate. TSG-6 = Tumour Necrosis Factor-inducible Gene 6. ECM = extracellular matrix. LV = left ventricular.

In this concept, aging serves as the host mechanism, where additional metabolic and mechanistic stress can operate via the same pathways by triggering and accelerating aging progression (**Figure 19**). We propose that metabolic and mechanical stress promote HFpEF development through the acceleration of aging at different levels. Hyperglycaemia and oxidative stress are two known factors of stress-induced premature cell senescence [84]. Together with the systemic inflammatory state, senescent cells contribute to the pro-inflammatory microenvironment of the heart and induce a microvascular endothelial inflammation [136]. This fits with the hypothesis of Paulus *et al*. in which endothelial inflammation is stated to reduce NO bioavailability, cGMP content and PKG activity at the onset of HFpEF [10] and with the observation that cGMP and PKG activity already lower with age alone [137]. In addition, hypertension is dependent, at least in part, of vascular NO bioavailability [138]. Visa versa, hypertension may thus contribute to endothelial dysfunction. Moreover, it has already been proposed that aging and hypertension may have similar cascades for the pathogenesis and development of endothelial dysfunction, highlighting their intertwined working [135]. We hypothesise that endothelial Pitx2 levels declines with age initiating microvascular regression. As a result, cardiac rarefaction contributes to alterations in the ECM matrix, resulting in remodelling and diastolic dysfunction, also seen in this project. Furthermore, mechanical stress resulting from hypertension additionally induces pressure overload in the heart, and earlier compensatory concentric LV hypertrophy with increased wall thickness [139].

This concept would imply the decoupling of endothelial Pitx2-loss-induced microvascular rarefaction from cardiomyocyte enlargement, which has indeed been evidenced in the *Pitx2*^{ECKO}. To further confirm this, endothelial Pitx2 expression levels can be measured over the course of aging with qPCR and IHC in hearts of old mice versus young animals. This concept would turn HFpEF pathology into a longevity question, opening a new window for the inhibition of senescence to prevent the HFpEF development.

Future improvements of the current model

In the near future, we want to investigate the role of endothelial Pitx2 deficiency in HFpEF development. We are therefore exposing adult *Pitx2*^{ECKO} mice to a HFD + L-NAME treatment instead of ablating Pitx2 at one week of age. We expect endothelial specific Pitx2 loss during adulthood to contribute majorly to the development of a HFpEF phenotype.

In the long term, we aim to combine the most accurate HFpEF model with Pitx2 endothelial overexpression, to rescue the disease phenotype of an appropriate HFpEF model. Both the *db/db* salt treated model and the HFD + L-NAME treatment on a C57BL/6J background have some critical limitations, while the aged model is the most physiological model of diastolic dysfunction but shows the mildest phenotype. Therefore, we will investigate a new mouse model, based on aged mice, with the addition of other HFpEF driving comorbidities. Several combinations are feasible. Firstly, aged mice treated with HFD + L-NAME can be examined upon accurate recapitulation of the HFpEF disease phenotype. Secondly, to mimic vessel regression during disease progression, the HFD + L-NAME treatment could be exchanged for a *Pitx2*^{ECKO} at older age. The conditional *Pitx2*^{ECKO} at an adult or semi-aged stage, would allow the rarefaction to act on the cardiac tissue over a longer time. Finally, we hypothesize that viral overexpression of endothelial Pitx2 in HFpEF model could rescue or decelerate disease progression elicited by, for example an extended HFD + L-NAME treatment. The method of overexpression was initiated for optimisation in this project, however, the *in vivo* experiments are still ongoing. The overexpression of endothelial Pitx2 is expected to rescue or at least ameliorate the disease presentation in a HFpEF mouse model. This would open the window for the creation of a Pitx2-based therapeutic strategy targeting HFpEF patients or for an early disease detection method where Pitx2 serves as a biological marker.

The proposed concept of aging as the backbone mechanism for HFpEF development accelerated by comorbidities supports the impossibility of an ‘ideal’ HFpEF model. Given the heterogeneity within the HFpEF comorbidities, any pre-clinical model will only represent a certain proportion of HFpEF patients. Similar to patients, a ‘one size-fits-all’ strategy in animal models is unlikely to succeed in a variable pathophysiology such as the HFpEF syndrome. The concept also emphasises that, although HFpEF is correlated with physiological dysregulations common to a modern western lifestyle, it is important not to disregard conserved pathways such as present in the ever-ongoing aging process. Therefore, interdisciplinary communication will be of utmost important in future pre-clinical research. Whether this is the best way to accomplish a therapeutic strategy for all human HFpEF patients remains an open question.

8 SAMENVATTING

Meer dan de helft van de hartfalenpatiënten worden gediagnostiseerd met Hart Falen met een preserveerde Ejectiefractie (HFpEF). HFpEF is een klinisch syndroom dat gekarakteriseerd wordt door verstijving van de cardiomyocyten, cardiale fibrose, hypertrofie en inflammatie, die de ontwikkeling van diastolische dysfunctie stimuleren. Zowel het systolische volume en het eind-diastolisch volume verminderen zodat de ejectiefractie constant blijft. Als een gevolg hiervan is het hart niet in staat om te voldoen aan de metabolische vraag van het lichaam. HFpEF patiënten kunnen minder goed fysieke inspanning verdragen, lijden aan longcongestie en perifeer oedeem, en hebben een hoog sterftecijfer.

Meer en meer wordt HFpEF aanzien als een systemische en progressieve ziekte, die ontstaat vanuit perifere risico factoren waarvan de effecten accumuleren in het hart, en leiden tot hartfalen. De comorbiditeiten die typisch geassocieerd zijn met HFpEF zoals een oudere leeftijd, obesitas, type 2 diabetes, hypertensie en nierfalen, drijven de ontwikkeling van HFpEF aan door het hart bloot te stellen aan oxidatieve en nitrosatieve stress. Hierdoor daalt de hoeveelheid biologisch beschikbaar stikstofmonoxide (NO) in de aangrenzende cardiomyocyten, wat op zijn beurt een hermodellering van het hartweefsel en diastolische dysfunctie veroorzaakt. Er werd recent een paradigma voorgesteld waarin de verstoorde NO-signalisatie in de cardiomyocyten de oorzaak zou van vergrootte en stijvere cardiomyocyten naarmate HFpEF ontwikkeld. De cluster aan comorbiditeiten en systemische inflammatie waarmee te patiënten kampen, worden ook verantwoordelijk geacht voor een stijging van zowel het aantal geïnfiltreerde immuun cellen en de verhoogde secretie van transforming growth factor β (TGF-β) in het myocardium, die samen de productie van fibrose weefsel stimuleren.

De exacte pathogenese van HFpEF blijft nog onduidelijk, hoewel de geobserveerde densiteitsdaling van de coronaire capillairen, ook wel rarefactie genoemd, verondersteld wordt een rol te spelen. Coronaire rarefactie komt voor in de comorbiditeiten die aan HFpEF voorafgaan, en is gecorreleerd met de typische hermodellering van het hartweefsel. Het onderzoek naar de pathogenese van HFpEF wordt echter tegengehouden door een gebrek aan geschikte diermodellen die de complexe heterogeniteit aan ziektebeelden bij patiënten nabootsen. Een eerste doelstelling in dit thesis project bestaat eruit om twee bestaande muismodellen (verouderde muizen en met zout behandelde *db/db* muizen) en één recent gepubliceerd muismodel (muizen gevoederd met een vetrijk dieet en L-NAME; HFD + L-NAME) te vergelijken om het best passende diermodel te identificeren. Het is noodzakelijk dat dit muismodel gemakkelijk genetisch modificeert kan worden, zodat ze kunnen ingezet worden in toekomstige experimenten die zich toespitsen op het mechanisme achterliggend aan rarefactie. Onze preliminaire data toonden gereduceerde expressie levels van *paired-like homeodomain transcription factor* 2 (Pitx2) in coronaire endotheelcellen aan, die samenviel met actieve capillaire regressie, en voorafging aan coronaire rarefactie. Pitx2 expressie is vereist voor asymmetrische ontwikkeling van bloedvaten tijdens embryogenese, en reguleert geprogrammeerde bloedvatregressie in de primordiale darm. We vermoeden dat het gebrek aan endotheelcel-specifieke expressie van Pitx2 regressie veroorzaakt van de coronaire capillairen met rarefactie als gevolg. Bijgevolg is het de tweede doelstelling van dit thesis project om deze hypothese te demonstreren met behulp van een conditioneel induceerbare *Pitx2*^{ECKO} muis.

Om het HFpEF fenotype van de drie muismodellen enerzijds en de *Pitx2*^{ECKO} muis anderzijds correct te evalueren, werden alle dieren onderzocht op afwijkingen in hun morfometrie en hartfunctie en op de hermodellering van het hart. Lichaams- en orgaangewicht werden genormaliseerd door lengte van de tibia. M-mode, *pulsed wave Doppler* en *tissue Doppler imaging* werden gebruikt om systolische en diastolische hypertrofie parameters vast te stellen. Verscheidene immunohistochemische en chemische kleuringen werden uitgevoerd op hartsecties om de verschillende aspecten van hartweefsel hermodellering te visualiseren.

We tonen hier aan dat *db/db* muizen die een zoutbehandeling kregen (*db/db* + S) het meest accuraat het HFpEF fenotype van patiënten recapituleren. Deze muizen waren het enige obese model en vertoonden het vergevorderde, restrictieve stadium van diastolische dysfunctie, gekoppeld aan coronaire capillaire rarefactie en vergrootte cardiomyocyten. De zoutbehandeling, versnelde daarom de ontwikkeling van diastolische dysfunctie, in vergelijking met onbehandelde *db/db* muizen. De HFD + L-NAME behandelde muizen vertoonden een pre-restrictieve fase van diastolische dysfunctie en de milde hermodellering van het hartweefsel waardoor hun fenotype minder goed overeenkwam met HFpEF dan aanvankelijk verwacht. Dit was waarschijnlijk te wijten aan de verschillende genetische achtergrond van ons model in vergelijking met de muizen gebruikt in de originele studie. De C57BL/6J achtergrond van onze muizen is gekend om zijn tragere gewichtstoename bij de consumptie van een vetrijk dieet, in vergelijking met de C57BL/6N achtergrond. Dit suggereert dat een verlengde HFD + L-NAME behandeling desalniettemin zou kunnen leiden tot een gepast HFpEF muismodel. Hoewel van alle geteste modellen de oude muizen de mildste vorm van diastolische dysfunctie vertoonden, was deze pseudonormale fase nog steeds ernstiger in vergelijking met diastolische dysfunctie in verouderingsmodellen die specifiek geselecteerd zijn voor hun leeftijds-geassocieerde afwijkingen. Dit impliceert dat gezonde veroudering op zichzelf een robuust mechanisme inhoudt, dat kan leiden tot de ontwikkeling van diastolische dysfunctie en hermodellering van het hartweefsel. Op basis van deze resultaten stellen we een concept voor waarin het verouderingsproces fungeert als de ruggengraat van HFpEF pathogenese. In gezonde omstandigheden is de levensduur te kort en kan het verouderingsproces niet lang genoeg inwerken op het hart. Wanneer het verouderingsproces getriggerd wordt door metabole of mechanische stress in de vorm van comorbiditeiten, wordt de veroudering van het hart extra gestimuleerd, resulterend in een meer gevorderd stadium van diastolische dysfunctie en cardiale hermodellering.

Een endotheel specifiek tekort aan Pitx2 in één week oude muizen induceerde, tegen onze verwachtingen in, eerder systolische dan diastolische dysfunctie. Deze discrepantie kan verklaard worden doordat regressie en rarefactie optraden terwijl hart nog aan het groeien was en de cardiomyocyten mitosis ondergingen. De rarefactie veroorzaakt door dit specifieke Pitx2 deficit beïnvloedde de uitbreiding van het aantal cardiomyocyten en resulteerde in een verminderde hartspiermassa en dilatatie. Om dit te omzeilen werd de timing van de conditionele Pitx2 deletie in een tweede experiment verlaat naar het adulte stadium. Op cellulair niveau demonstreerden de *Pitx2*^{ECKO} muizen coronaire capillaire rarefactie ontkoppeld van cardiomyocyt hypertrofie. Velen geloven dat het densiteitsverlies aan hartcapillairen enkel secundair aan cardiomyocyt vergroting optreedt. Samen met dit resultaat, toont recent bewijs echter aan dat een actief proces voorafgaat aan hypertrofie. Dit ondersteunt de brede hypothese dat coronaire capillaire rarefactie op zijn minst gedeeltelijk verantwoordelijk is voor hermodellering van het hartweefsel tijdens de ontwikkeling van HFpEF, ook al vertoonde onze 1 week oude *Pitx2*^{ECKO} muizen geen HFpEF fenotype. In tegenstelling tot rarefactie kon actieve bloedvatregressie niet gedetecteerd worden in

het hart van de *Pitx2*^{ECKO} muizen. Bloedvatregressie is echter slechts een kortstondig event waardoor het waarschijnlijk gemist werd op het moment van de analyse. Bijgevolg blijft ook de hypothese waarin actieve bloedvatregressie de oorzaak is van rarefactie die ook voorkomt bij HFpEF patiënten, nog steeds plausibel.

Enkele toekomstige verbeteringen van het huidige model kunnen voorgesteld worden op basis van de interpretatie van resultaten verworven in dit thesis project. De HFD + L-NAME behandeling kan gebruikt worden als extra stimulans in het verouderingsmodel. Endotheel-specifiek verlies van Pitx2 expressie op de leeftijd van 1 week kon geen HFpEF fenotype veroorzaken, en een tweede experiment waarbij Pitx2 pas conditioneel verwijderd wordt op adulte leeftijd is nog aan de gang. We vermoeden desondanks dat een endotheel Pitx2 tekort op de leeftijd van 7 weken, net als HFD + L-NAME behandeling, HFpEF ontwikkeling zal stimuleren in oude muizen. Om de directe invloed van endotheel-specifieke Pitx2 deficiëntie te testen op HFpEF pathogenese, zal Pitx2 conditioneel geëlimineerd worden in adulte *Pitx2*^{ECKO} muizen behandeld met HFD en L-NAME. Het doel op lange termijn bestaat eruit om het HFpEF fenotype van een gepast muismodel te reverseren door Pitx2 viraal te overexpressie te brengen in het endotheel.

9 ACKNOWLEDGEMENTS

First and foremost, I want to thank my promotor Prof. Jones. Liz, thank you for giving me the opportunity to start my thesis in your lab, even though I studied at another university and had no biomedical background at first. I was very delighted and grateful to become a member of the JonesLab and I hope my work has been worthy of your trust. I also want to thank the whole research group for making my stay so enjoyable, for having your doors always open, and to infect me with your enthusiasm for cardiovascular research.

Thanks to Bram, Ashkan, and Paolo for the various hungry walks to the 'limoen' or to fill my evenings with extraordinary theatre. To Nadèche for your excellent echo work and to show me again and again were stuff lives in the lab. I hope we can go buy some plants together soon to the decorate the office. To Ilona for your daily hilarious stories. To read my writings and to be always willing to give a helping hand. To Hanna, for introducing me to crack muffins and for your contagious everyday cheerfulness. For meeting my high fives when I received good news and a listening ear when in case of bad. To Margo, both thanks and not so much thanks to set the standard for students this high, for reading my thesis and to push me for better. For taking me on walks through Leuven's fields, to calm me down when I panicked over deadlines, and just to become a really good friend. Cheers to all our future nerdy talks and collaborations.

To my parents, for their flexibility and eternal support in my education and everything next to it. To my dearest friends, for listening to my weird stories about mice and lab work, for the various encouraging phone calls to Ghent when I needed them and for all our crazy events. You are the most wonderful friends one could wish for. To Ellen, for the banding while making word puzzles or waiting for the next washing step. For introducing me to Wannes, for your enormous hospitality and save me from loneliness during the covid-lockdown. For becoming my virus buddy that understands me with only a whale or a flag. For the bottles of soda we shared at quiet mature evenings that always made return back home before dusk. Bamboozled again. For teaching me that anyone can become family as long as you give them love and enough food. You are both a scientist and a woman to look up to.

And finally, to my supervisor Steve. For teaching me too much to list here and offering so much of your time. For your clear explanations that never missed a nuance, for reading the FWO application and manuscripts before I even started my thesis. For teaching me proper lab skills and to ensure me that there wasn't any question too stupid to ask (yet I succeeded to find them). I was extremely lucky with a supervisor like you and there will always reside a little part of Dr. Simmonds' advise in my future research. A heartfelt thank you.

Jana

10 REFERENCES

[1] L. S. Athanasiou, D. I. Fotiadis, and L. K. Michalis, "Introduction," in *Atherosclerotic Plaque Characterization Methods Based on Coronary Imaging*, 1st Editio., Academic Press, 2017, pp. 1–21.

[2] C. D. Kemp and J. V. Conte, "The pathophysiology of heart failure," *Cardiovasc. Pathol.*, vol. 21, no. 5, pp. 365–371, 2012.

[3] P. Ponikowski *et al.*, "Heart failure: Preventing disease and death worldwide," *ECS Hear. Fail.*, vol. 1, no. 1, pp. 4–25, 2014.

[4] S. S. Najjar, "Heart Failure with Preserved Ejection Fraction: Failure to Preserve, Failure of Reserve, and Failure on the Compliance Curve," *J Am Coll Cardiol*, vol. 54, no. 5, pp. 419–421, 2009.

[5] B. A. Steinberg *et al.*, "Health Services and Outcomes Research Trends in Patients Hospitalized With Heart Failure and Prevalence , Therapies , and Outcomes," 2012.

[6] M. A. Konstam and F. M. Abboud, "Ejection Fraction: Misunderstood and Overrated (Changing the Paradigm in Categorizing Heart Failure)," *Circulation*, vol. 135, no. 8, pp. 717–719, 2017.

[7] E. E. S. Van Riet, A. W. Hoes, K. P. Wagenaar, A. Limburg, M. A. J. Landman, and F. H. Rutten, "Epidemiology of heart failure: the prevalence of heart failure and ventricular dysfunction in older adults over time. A systematic review," *Rev. Port. Cardiol.*, vol. 36, no. 5, pp. 405–407, 2017.

[8] J. E. Wilcox *et al.*, "Factors associated with improvement in ejection fraction in clinical practice among patients with heart failure: Findings from IMPROVE HF," *Am. Heart J.*, vol. 163, no. 1, pp. 49-56.e2, 2012.

[9] M. Valero-Muñoz, W. Backman, and F. Sam, "Murine Models of Heart Failure With Preserved Ejection Fraction: A 'Fishing Expedition,'" *JACC Basic to Transl. Sci.*, vol. 2, no. 6, pp. 770–789, 2017.

[10] W. J. Paulus and C. Tschöpe, "A novel paradigm for heart failure with preserved ejection fraction: Comorbidities drive myocardial dysfunction and remodeling through coronary microvascular endothelial inflammation," *J. Am. Coll. Cardiol.*, vol. 62, no. 4, pp. 263–271, 2013.

[11] T. E. Owan, D. O. Hodge, R. M. Herges, S. J. Jacobsen, V. L. Roger, and M. M. Redfield, "Trends in prevalence and outcome of heart failure with preserved ejection fraction," *N. Engl. J. Med.*, vol. 355, no. 3, pp. 251–259, 2006.

[12] C. S. P. Lam, E. Donal, E. Kraigher-Krainer, and R. S. Vasan, "Epidemiology and clinical course of heart failure with preserved ejection fraction," *Eur. J. Heart Fail.*, vol. 13, no. 1, pp. 18–28, 2011.

[13] M. Tadic, C. Cuspidi, S. Plein, E. Belyavskiy, F. Heinzel, and M. Galderisi, "Sex and Heart Failure with Preserved Ejection Fraction: From Pathophysiology to Clinical Studies," *J. Clin. Med.*, vol. 8, no. 6, p. 792, 2019.

[14] F. Braunschweig, M. R. Cowie, and A. Auricchio, "What are the costs of heart failure?," *Europace*, vol. 13, no. SUPPL. 2, pp. 13–17, 2011.

[15] S. Maréchaux *et al.*, "Prognostic importance of comorbidities in heart failure with preserved left ventricular ejection fraction," *Heart Vessels*, vol. 26, no. 3, pp. 313–320, 2011.

[16] C. Ergatoudes, M. Schaufelberger, B. Andersson, A. Pivodic, U. Dahlström, and M. Fu, "Non-cardiac comorbidities and mortality in patients with heart failure with reduced vs. preserved ejection fraction: a study using the Swedish Heart Failure Registry," *Clin. Res. Cardiol.*, vol. 108, no. 9, pp. 1025–1033, 2019.

[17] Sameer Ather *et al.*, "Impact of Non-Cardiac Comorbidities on Morbidity and Mortality in a Predominantly Male Population with Heart Failure and Preserved versus Reduced Ejection Fraction," *J Am Coll Cardiol*, vol. 59, no. 11, pp. 998–1005, 2012.

[18] D. S. Lee *et al.*, "Relation of disease pathogenesis and risk factors to heart failure with preserved or reduced ejection fraction: Insights from the framingham heart study of the national heart, lung, and blood institute," *Circulation*, vol. 119, no. 24, pp. 3070–3077, 2009.

[19] R. B. Devereux *et al.*, "Echocardiographic assessment of left ventricular hypertrophy: Comparison to necropsy findings," *Am. J. Cardiol.*, vol. 57, no. 6, pp. 450–458, 1986.

[20] D. Zipes and P. Libby, *Braunwald's Heart Disease: A Textbook of Cardiovascular Medicine*, 11th Editi. Elsevier, 2018.

[21] C. Y. Ho, "Echocardiographic Assessment of Diastolic Function," in *Contemporary Cardiology: Essential Echocardiography: A Practical Handbook With DVD*, Totowa, NJ: Humana Press, 2007, pp. 119–120.

[22] E. Dal Canto *et al.*, "Diagnostic value of echocardiographic markers for diastolic dysfunction and heart failure with preserved ejection fraction," *Heart Fail. Rev.*, 2020.

[23] G. L. J. Vermeiren, M. L. N. G. Malbrain, and J. M. J. B. Walpot, "Cardiac Ultrasonography in the critical care setting: a practical approach to asses cardiac function and preload for the 'non-cardiologist,'" *Anaesthesiol. Intensive Ther.*, vol. 47, pp. 89–104, 2015.

[24] M. J. Garcia, J. D. Thomas, and A. L. Klein, "New Doppler Echocardiographic Applications for the Study of Diastolic Function," *J. Am. Coll. Cardiol.*, vol. 32, no. 4, pp. 865–875, 1998.

[25] A. E. Huis in 't Veld, F. S. de Man, A. C. van Rossum, and M. L. Handoko, "How to diagnose heart failure with preserved ejection fraction: The value of invasive stress testing," *Netherlands Hear. J.*, vol. 24, no. 4, pp. 244–251, 2016.

[26] M. R. Zile *et al.*, "Myocardial Stiffness in Patients with Heart Failure and a Preserved Ejection Fraction: Contributions of

Collagen and Titin," *Circulation*, vol. 131, no. 14, pp. 1247–1259, 2015.
[27] M. Kasner *et al.*, "Diastolic tissue doppler indexes correlate with the degree of collagen expression and cross-linking in heart failure and normal ejection fraction," *J. Am. Coll. Cardiol.*, vol. 57, no. 8, pp. 977–985, 2011.
[28] S. J. Simmonds, I. Cuijpers, and S. Heymans, "Cellular and Molecular Di ff erences between HFpEF and HFrEF : A Step Ahead in an Improved," *Cells*, vol. 9, p. 242, 2020.
[29] K. T. Weber, "Cardiac interstitium in health and disease: The fibrillar collagen network," *J. Am. Coll. Cardiol.*, vol. 13, no. 7, pp. 1637–1652, 1989.
[30] M. Shi *et al.*, "Latent TGF-Beta structure and activation," *Nature*, vol. 474, no. 3, pp. 343–349, 2011.
[31] A. Bielecka-Dabrowa *et al.*, "Differences in biochemical and genetic biomarkers in patients with heart failure of various etiologies," *Int. J. Cardiol.*, vol. 221, pp. 1073–1080, 2016.
[32] J. Baum and H. S. Duffy, "Fibroblasts and Myofibroblasts: What are we talking about?," *J. Cardiovasc. Pharmacol.*, vol. 57, no. 4, pp. 376–379, 2011.
[33] A. González, S. Ravassa, J. Beaumont, B. López, and J. Díez, "New targets to treat the structural remodeling of the myocardium," *J. Am. Coll. Cardiol.*, vol. 58, no. 18, pp. 1833–1843, 2011.
[34] D. Westermann *et al.*, "Role of left ventricular stiffness in heart failure with normal ejection fraction," *Circulation*, vol. 117, no. 16, pp. 2051–2060, 2008.
[35] C. M. Warren, M. C. Jordan, K. P. Roos, P. R. Krzesinski, and M. L. Greaser, "Titin isoform expression in normal and hypertensive myocardium," *Cardiovasc. Res.*, vol. 59, no. 1, pp. 86–94, 2003.
[36] N. Hamdani, K. G. Bishu, M. Von Frieling-Salewsky, M. M. Redfield, and W. A. Linke, "Deranged myofilament phosphorylation and function in experimental heart failure with preserved ejection fraction," *Cardiovasc. Res.*, vol. 97, no. 3, pp. 464–471, 2013.
[37] K. E. Runte *et al.*, "Relaxation and the Role of Calcium in Isolated Contracting Myocardium From Patients With Hypertensive Heart Disease and Heart Failure With Preserved Ejection Fraction.," *Circ Hear. Fail.*, vol. 10, no. 8, 2017.
[38] L. van Heerebeek, "Impact of Comorbidities on Myocardial Remodeling and Dysfunction In Heart Failure with Preserved Ejection Fraction," *SOJ Pharm. Pharm. Sci.*, vol. 1(2), no. 20, 2014.
[39] A. R. Marks and A. R. Marks, "Calcium and the heart : a question of life and death Find the latest version : Calcium and the heart : a question of life and death," vol. 111, no. 5, pp. 597–600, 2003.
[40] C. Franssen and A. González Miqueo, "The role of titin and extracellular matrix remodelling in heart failure with preserved ejection fraction," *Netherlands Hear. J.*, vol. 24, no. 4, pp. 259–267, 2016.
[41] L. Van Heerebeek *et al.*, "Myocardial structure and function differ in systolic and diastolic heart failure," *Circulation*, vol. 113, no. 16, pp. 1966–1973, 2006.
[42] L. Van Heerebeek *et al.*, "Low myocardial protein kinase G activity in heart failure with preserved ejection fraction," *Circulation*, vol. 126, no. 7, pp. 830–839, 2012.
[43] W. J. Paulus and C. Tschöpe, "A novel paradigm for heart failure with preserved ejection fraction: Comorbidities drive myocardial dysfunction and remodeling through coronary microvascular endothelial inflammation," *J. Am. Coll. Cardiol.*, vol. 62, no. 4, pp. 263–271, 2013.
[44] A. Desai and J. C. Fang, "Heart Failure with Preserved Ejection Fraction: Hypertension, Diabetes, Obesity/Sleep Apnea, and Hypertrophic and Infiltrative Cardiomyopathy," *Heart Fail. Clin.*, vol. 4, no. 1, pp. 87–97, 2008.
[45] E. Takimoto *et al.*, "Chronic inhibition of cyclic GMP phosphodiesterase 5A prevents and reverses cardiac hypertrophy," *Nat. Med.*, vol. 11, no. 2, pp. 214–222, 2005.
[46] D. Westermann *et al.*, "Cardiac inflammation contributes to changes in the extracellular matrix in patients with heart failure and normal ejection fraction," *Circ. Hear. Fail.*, vol. 4, no. 1, pp. 44–52, 2011.
[47] R. D. E. Vito *et al.*, "Markers of activated inflammatory cells correlate with severity of liver damage in children with nonalcoholic fatty liver disease," *Int. J. Mol. Med.*, vol. 30, no. 1, pp. 49–56, 2012.
[48] A. Nakanos, T. Harada, and S. Morikawa, "Expression of Leukocyte Common Antigen (CD45) on Various Human Leukemia / Lymphoma Cell Lines," *Acta Pathol Jpn*, vol. 40, no. 2, pp. 107–115, 1990.
[49] S. J. Shah, "Matchmaking for the optimization of clinical trials of heart failure with preserved ejection fraction: No laughing matter," *J. Am. Coll. Cardiol.*, vol. 62, no. 15, pp. 1339–1342, 2013.
[50] S. A. Doggrell and L. Brown, "Rat models of hypertension, cardiac hypertrophy and failure," *Cardiovasc. Res.*, vol. 39, no. 1, pp. 89–105, 1998.
[51] K. A. Griffin, M. Abu-Naser, I. Abu-Amarah, M. Picken, G. A. Williamson, and A. K. Bidani, "Dynamic blood pressure load and nephropathy in the ZSF1 (fa/fa cp) model of type 2 diabetes," *Am. J. Physiol. - Ren. Physiol.*, vol. 293, no. 5, pp. 1605–1613, 2007.
[52] N. Hamdani *et al.*, "Left ventricular diastolic dysfunction and myocardial stiffness in diabetic mice is attenuated by inhibition of dipeptidyl peptidase 4," *Cardiovasc. Res.*, vol. 104, no. 3, pp. 423–431, 2014.
[53] N. Hamdani *et al.*, "Myocardial titin hypophosphorylation importantly contributes to heart failure with preserved ejection fraction in a rat metabolic risk model," *Circ. Hear. Fail.*, vol. 6, no. 6, pp. 1239–1249, 2013.
[54] C. G. M. Van Dijk *et al.*, "Distinct endothelial cell responses in the heart and kidney microvasculature characterize the

progression of heart failure with preserved ejection fraction in the obese ZSF1 rat with cardiorenal metabolic syndrome," *Circ. Hear. Fail.*, vol. 9, no. 4, pp. 1–13, 2016.
[55] S. J. Burke *et al.*, "db / db Mice Exhibit Features of Human Type 2 Diabetes That Are Not Present in Weight-Matched C57BL / 6J Mice Fed a Western Diet," *J. Diabetes Res.*, vol. Article ID, 2017.
[56] L. A. Barouch, D. E. Berkowitz, R. W. Harrison, C. P. O'Donnell, and J. M. Hare, "Disruption of leptin signaling contributes to cardiac hypertrophy independently of body weight in mice," *Circulation*, vol. 108, no. 6, pp. 754–759, 2003.
[57] H. Cucak, L. G. Grunnet, and A. Rosendahl, "Accumulation of M1-like macrophages in type 2 diabetic islets is followed by a systemic shift in macrophage polarization," *J. Leukoc. Biol.*, vol. 95, no. 1, pp. 149–160, 2014.
[58] J. C. Reil *et al.*, "Heart rate reduction by If-inhibition improves vascular stiffness and left ventricular systolic and diastolic function in a mouse model of heart failure with preserved ejection fraction," *Eur. Heart J.*, vol. 34, no. 36, pp. 2839–2849, 2013.
[59] J. E. Ostler *et al.*, "Effects of insulin resistance on skeletal muscle growth and exercise capacity in type 2 diabetic mouse models," *Am. J. Physiol. - Endocrinol. Metab.*, vol. 306, no. 6, pp. 592–605, 2014.
[60] A. M. Papinska, M. Soto, and and K. E. R. , Christopher J. Meeks, "Long-term administration of angiotensin (1-7) prevents heart and lung dysfunction in a mouse model of type 2 diabetes (db/db) by reducing oxidative stress, inflammation and pathological remodeling," *Physiol. Behav.*, vol. 176, no. 10, pp. 139–148, 2017.
[61] T. L. Broderick, M. Jankowski, D. Wang, B. A. Danalache, C. R. Parrott, and J. Gutkowska, "Downregulation in GATA4 and Downstream Structural and Contractile Genes in the db/db Mouse Heart," *ISRN Endocrinol.*, vol. 2012, pp. 1–12, 2012.
[62] G. G. Schiattarella *et al.*, "Nitrosative stress drives heart failure with preserved ejection fraction," *Nature*, vol. 568, no. 7752, pp. 351–356, 2019.
[63] Jana Kopincová, Angelika Púzserová, and Iveta Bernátová, "L-NAME in the cardiovascular system – nitric oxide synthase activator?," *Pharmacol. Reports*, vol. 64, no. 3, pp. 511–520, 2012.
[64] L. Paulis *et al.*, "Regression of L-NAME-induced hypertension: The role of nitric oxide and endothelium-derived constricting factor," *Hypertens. Res.*, vol. 31, no. 4, pp. 793–803, 2008.
[65] T. R. Sahrawat and D. Chatterjee, "Time-Dependent Model to Mimic Acetylcholine Induced Vasodilatation in Arterial Smooth Muscle Cells," *Int. Lett. Nat. Sci.*, vol. 52, pp. 60–66, 2016.
[66] Y. Zhou, S. Varadharaj, X. Zhao, N. Parinandi, N. A. Flavahan, and J. L. Zweier, "Acetylcholine causes endothelium-dependent contraction of mouse arteries," *Am. J. Physiol. - Hear. Circ. Physiol.*, vol. 289, no. 3 58-3, pp. 1027–1032, 2005.
[67] M. M. Simon *et al.*, "A comparative phenotypic and genomic analysis of C57BL/6J and C57BL/6N mouse strains," *Genome Biol.*, vol. 14, no. 7, pp. 1–22, 2013.
[68] A. L. Reed *et al.*, "Diastolic dysfunction is associated with cardiac fibrosis in the senescence-accelerated mouse," *Am. J. Physiol. - Hear. Circ. Physiol.*, vol. 301, no. 3, pp. 824–831, 2011.
[69] V. Karuppagounder *et al.*, "The senescence accelerated mouse prone 8 (SAMP8): A novel murine model for cardiac aging," *Ageing Res. Rev.*, vol. 35, pp. 291–296, 2017.
[70] S. F. Mohammed, S. Hussain, S. A. Mirzoyev, W. D. Edwards, J. J. Maleszewski, and M. M. Redfield, "Coronary Microvascular Rarefaction and Myocardial Fibrosis in Heart Failure with Preserved Ejection Fraction," *Circulation.*, vol. 131, no. 6, pp. 550–559, 2015.
[71] M. S. Goligorsky, "Microvascular rarefaction: The decline and fall of blood vessels," *Organogenesis*, vol. 6, no. 1, pp. 1–10, 2010.
[72] B. I. Lévy, "Microvascular plasticity and experimental heart failure," *Hypertension*, vol. 47, no. 5, pp. 827–829, 2006.
[73] J. P. Noon *et al.*, "Impaired microvascular dilatation and capillary rarefaction in young adults with a predisposition to high blood pressure," *J. Clin. Invest.*, vol. 99, no. 8, pp. 1873–1879, 1997.
[74] C. Cheng, J. J. Diamond, and B. Falkner, "Functional Capillary Rarefaction in Mild Blood Pressure Elevation," *Clin. Transl. Sci.*, vol. 1, no. 1, pp. 75–79, 2008.
[75] J. S. Bonner, L. Lantier, C. M. Hasenour, F. D. James, D. P. Bracy, and D. H. Wasserman, "Muscle-specific vascular endothelial growth factor deletion induces muscle capillary rarefaction creating muscle insulin resistance," *Diabetes*, vol. 62, no. 2, pp. 572–580, 2013.
[76] S. Rattigan, S. M. Richards, and M. A. Keske, "Microvascular contributions to insulin resistance," *Diabetes*, vol. 62, no. 2, pp. 343–345, 2013.
[77] M. Nieuwdorp *et al.*, "Loss of endothelial glycocalyx during acute hyperglycemia coincides with endothelial dysfunction and coagulation activation in vivo," *Diabetes*, vol. 55, no. 2, pp. 480–486, 2006.
[78] C. Korn and H. G. Augustin, "Mechanisms of Vessel Pruning and Regression," *Dev. Cell*, vol. 34, no. 1, pp. 5–17, 2015.
[79] P. Baluk, S. Morikawa, A. Haskell, M. Mancuso, and D. M. Mcdonald, "Abnormalities of Basement Membrane on Blood Vessels and Endothelial Sprouts in Tumors," vol. 163, no. 5, pp. 1801–1815, 2003.
[80] D. S. GRANT, H. K. KLEINMAN, and G. R. MARTIN, "The Role of Basement Membranes in Vascular Development," *Ann. N. Y. Acad. Sci.*, vol. 588, no. 1, pp. 61–72, 1990.
[81] F. Baffert *et al.*, "Cellular changes in normal blood capillaries undergoing regression after inhibition of VEGF signaling," *Am. J. Physiol. - Hear. Circ. Physiol.*, vol. 290, no. 2, pp. 547–559, 2006.

[82] W. E. SONNTAG, C. LYNCH, P. THORNTON, A. KHAN, S. BENNETT, and R. INGRAM, "The effects of growth hormone and IGF-1 deficiency on cerebrovascular and brain ageing," *J. Anat.*, vol. 197, no. 4, pp. 575–585, 2000.
[83] Y. Izumiya, I. Shiojima, K. Sato, D. B. Sawyer, W. S. Colucci, and K. Walsh, "Vascular endothelial growth factor blockade promotes the transition from compensatory cardiac hypertrophy to failure in response to pressure overload," *Hypertension*, vol. 47, no. 5, pp. 887–893, 2006.
[84] H. Shakeri *et al.*, "Neuregulin-1 attenuates stress-induced vascular senescence," *Cardiovasc. Res.*, vol. 114, no. 7, pp. 1041–1051, 2018.
[85] H. Zeng and J. X. Chen, "Microvascular Rarefaction and Heart Failure With Preserved Ejection Fraction," *Front. Cardiovasc. Med.*, vol. 6, no. 15, pp. 1–7, 2019.
[86] H. Zeng and J. X. Chen, "Sirtuin 3, Endothelial Metabolic Reprogramming, and Heart Failure with Preserved Ejection Fraction," *J. Cardiovasc. Pharmacol.*, vol. 74, no. 4, pp. 315–323, 2019.
[87] D. Franco, D. Sedmera, and E. Lozano-Velasco, "Multiple Roles of Pitx2 in Cardiac Development and Disease," *J. Cardiovasc. Dev. Dis.*, vol. 4, no. 4, p. 16, 2017.
[88] H. Hamada, C. Meno, D. Watanabe, and Y. Saijoh, "Establishment of vertebrate left-right asymmetry," *Nat. Rev. Genet.*, vol. 3, no. 2, pp. 103–113, 2002.
[89] K. Kitamura *et al.*, "Mouse Pitx2 deficiency leads to anomalies of the ventral body wall, heart, extra- and periocular mesoderm and right pulmonary isomerism," *Development*, vol. 126, no. 24, pp. 5749–5758, 1999.
[90] C. Kioussi *et al.*, "Identification of a WntDv-Catenin → Pitx2 Pathway.pdf," *Cell*, vol. 111, no. 5, pp. 673–685, 2011.
[91] M.-F. Lu, C. Pressman, R. Dyer, R. L. Johnson, and J. F. Martin, "Function of Rieger syndrome gene in left-right asymmetry and craniofacial development," *Nature*, vol. 401, pp. 276–278, 1999.
[92] A. Chinchilla *et al.*, "PITX2 insufficiency leads to atrial electrical and structural remodeling linked to arrhythmogenesis," *Circ. Cardiovasc. Genet.*, vol. 4, no. 3, pp. 269–279, 2011.
[93] A. Sivakumar *et al.*, "Midgut Laterality Is Driven by Hyaluronan on the Right," *Dev. Cell*, vol. 46, no. 5, pp. 533-551.e5, 2018.
[94] A. Mahadevan *et al.*, "The Left-Right Pitx2 Pathway Drives Organ-Specific Arterial and Lymphatic Development in the Intestine," *Dev. Cell*, vol. 31, no. 6, pp. 690–706, 2014.
[95] C. Liu, W. Liu, J. Palie, M. F. Lu, N. A. Brown, and J. F. Martin, "Pitx2c patterns anterior myocardium and aortic arch vessels and is required for local cell movement into atrioventricular cushions," *Development*, vol. 129, no. 21, pp. 5081–5091, 2002.
[96] K. Yashiro, H. Shiratori, and H. Hamada, "Haemodynamics determined by a genetic programme govern asymmetric development of the aortic arch," *Nature*, vol. 450, no. 7167, pp. 285–288, 2007.
[97] M. Durbeej, "Laminins," *Cell Tissue Res.*, vol. 339, pp. 259–268, 2010.
[98] L. Alex, I. Russo, V. Holoborodko, and N. G. Frangogiannis, "Characterization of a mouse model of obesity-related fibrotic cardiomyopathy that recapitulates features of human heart failure with preserved ejection fraction," *Am. J. Physiol. - Hear. Circ. Physiol.*, vol. 315, no. 4, pp. H934–H949, 2018.
[99] K. Hirata *et al.*, "Exendin-4 has an anti-hypertensive effect in salt-sensitive mice model," *Biochem. Biophys. Res. Commun.*, vol. 380, no. 1, pp. 44–49, 2009.
[100] H. Hackbarth and D. E. Harrison, "Changes with age in renal function and morphology in C57BL/6, CBA/HT6, and B6CBAF1 mice," *Journals Gerontol.*, vol. 37, no. 5, pp. 540–547, 1982.
[101] A. Fahlström, Q. Yu, and B. Ulfhake, "Behavioral changes in aging female C57BL/6 mice," *Neurobiol. Aging*, vol. 32, no. 10, pp. 1868–1880, 2011.
[102] S. Y. Li *et al.*, "Aging induces cardiac diastolic dysfunction, oxidative stress, accumulation of advanced glycation endproducts and protein modification," *Aging Cell*, vol. 4, no. 2, pp. 57–64, 2005.
[103] M. W. Hamrick *et al.*, "Age-related loss of muscle mass and bone strength in mice is associated with a decline in physical activity and serum leptin," *Bone*, vol. 39, no. 4, pp. 845–853, 2006.
[104] K. H. Fisher-Wellman *et al.*, "A direct comparison of metabolic responses to high-fat diet in c57bl/6j and c57bl/6nj mice," *Diabetes*, vol. 65, no. 11, pp. 3249–3261, 2016.
[105] G. A. Bray and J. Macdiarmid, "The epidemic of obesity and diabetes," *West. J. Med.*, vol. 172, no. 2, pp. 78–79, 2000.
[106] A. L. Reed *et al.*, "Diastolic dysfunction is associated with cardiac fibrosis in the senescence-accelerated mouse," no. 12, pp. 824–831, 2019.
[107] G. E. Taffet, C. J. Hartley, X. Wen, T. Pham, L. H. Michael, and M. L. Entman, "Noninvasive indexes of cardiac systolic and diastolic function in hyperthyroid and senescent mouse," *Am. J. Physiol. - Hear. Circ. Physiol.*, vol. 270, no. 6 39-6, 1996.
[108] J. Mori *et al.*, "Angiotensin 1-7 ameliorates diabetic cardiomyopathy and diastolic dysfunction in db/db mice by reducing lipotoxicity and inflammation," *Circ. Hear. Fail.*, vol. 7, no. 2, pp. 327–339, 2014.
[109] A. Van den Bergh, W. Flameng, and P. Herijgers, "Type II diabetic mice exhibit contractile dysfunction but maintain cardiac output by favourable loading conditions," *Eur. J. Heart Fail.*, vol. 8, no. 8, pp. 777–783, 2006.
[110] D. J. Campbell *et al.*, "Obesity is associated with lower coronary microvascular density," *PLoS One*, vol. 8, no. 11, pp. 7–9, 2013.

[111] W. P. Cheol *et al.*, "Vascular endothelial growth factor inhibition by dRK6 causes endothelial apoptosis, fibrosis, and inflammation in the heart via the Akt/eNOS Axis in db/db mice," *Diabetes*, vol. 58, no. 11, pp. 2666–2676, 2009.
[112] E. Plante, A. Menaouar, B. A. Danalache, T. L. Broderick, M. Jankowski, and J. Gutkowska, "Treatment with brain natriuretic peptide prevents the development of cardiac dysfunction in obese diabetic db/db mice," *Diabetologia*, vol. 57, no. 6, pp. 1257–1267, 2014.
[113] A. Fraticelli, R. Josephson, R. Danziger, E. Lakatta, and H. Spurgeon, "Morphological and contractile characteristics of rat cardiac myocytes from maturation to senescence," *Am. J. Physiol. - Hear. Circ. Physiol.*, vol. 257, no. 1, 1989.
[114] D. F. Dai and P. S. Rabinovitch, "Cardiac Aging in Mice and Humans: The Role of Mitochondrial Oxidative Stress," *Trends Cardiovasc. Med.*, vol. 19, no. 7, pp. 213–220, 2009.
[115] F. P. Brouwers *et al.*, "Incidence and epidemiology of new onset heart failure with preserved vs. reduced ejection fraction in a community-based cohort: 11-year follow-up of PREVEND," *Eur. Heart J.*, vol. 34, no. 19, pp. 1424–1431, 2013.
[116] A. H. Chaanine *et al.*, "FOXO3A regulates BNIP3 and modulates mitochondrial calcium, dynamics, and function in cardiac stress," *Am. J. Physiol. - Hear. Circ. Physiol.*, vol. 311, no. 6, pp. H1540–H1559, 2016.
[117] K. Rakusan and J. Nagai, "Morphometry of arterioles and capillaries in hearts of senescent mice," *Cardiovasc. Res.*, vol. 28, no. 7, pp. 969–972, 1994.
[118] P. Anversa, P. Li, E. H. Sonnenblick, and G. Olivetti, "Effects of aging on quantitative structural properties of coronary vasculature and microvasculature in rats," *Am. J. Physiol. - Hear. Circ. Physiol.*, vol. 267, no. 3 36-3, 1994.
[119] N. Scherbakov *et al.*, "Insulin resistance in heart failure: Differences between patients with reduced and preserved left ventricular ejection fraction," *Eur. J. Heart Fail.*, vol. 17, no. 10, pp. 1015–1021, 2015.
[120] E. Konduracka, A. Gackowski, P. Rostoff, D. Galicka-Latala, W. Frasik, and W. Piwowarska, "Diabetes-specific cardiomyopathy in type 1 diabetes mellitus: No evidence for its occurrence in the era of intensive insulin therapy," *Eur. Heart J.*, vol. 28, no. 20, pp. 2465–2471, 2007.
[121] A. Grillo, L. Salvi, P. Coruzzi, P. Salvi, and G. Parati, "Sodium intake and hypertension," *Nutrients*, vol. 11, no. 9, pp. 1–16, 2019.
[122] M. Cikes, "Dilated Cardiomyopathies," in *Essential Echocardiography: A Companion to Braunwald's Heart Disease*, vol. 219, no. Dcm, Elsevier, 2019, pp. 219-229.e1.
[123] K. Alkass, J. Panula, M. Westman, T. Di Wu, J. L. Guerquin-Kern, and O. Bergmann, "No Evidence for Cardiomyocyte Number Expansion in Preadolescent Mice," *Cell*, vol. 163, no. 4, pp. 1026–1036, 2015.
[124] C. Perrino *et al.*, "Intermittent pressure overload triggers hypertrophy-independent cardiac dysfunction and vascular rarefaction," *J. Clin. Invest.*, vol. 116, no. 6, pp. 1547–1560, 2006.
[125] L. Ferrucci, "The Baltimore Longitudinal Study of Aging (BLSA): A 50-Year-Long Journey and Plans for the Future," *Journals Gerontol. Ser. A*, vol. 63, no. 12, pp. 1416–1419, 2008.
[126] V. Adams *et al.*, "High-intensity interval training attenuates endothelial dysfunction in a Dahl salt-sensitive rat model of heart failure with preserved ejection fraction," *J. Appl. Physiol.*, vol. 119, no. 6, pp. 745–752, 2015.
[127] E. G. Lakatta, "Arterial and cardiac aging: Major shareholders in cardiovascular disease enterprises. Part III: Cellular and molecular clues to heart and arterial aging," *Circulation*, vol. 107, no. 3, pp. 490–497, 2003.
[128] E. G. Lakatta and D. Levy, "Arterial and cardiac aging: Major shareholders in cardiovascular disease enterprises: Part II: The aging heart in health: Links to heart disease," *Circulation*, vol. 107, no. 2, pp. 346–354, 2003.
[129] L. de las Fuentes *et al.*, "Effect of moderate diet-induced weight loss and weight regain on cardiovascular structure and function," *Cardiopulm. Phys. Ther. A Guid. to Pract. Fourth Ed.*, vol. 54, no. 25, pp. 3–38, 2004.
[130] S. Nanayakkara and D. M. Kaye, "Management of Heart Failure with Preserved Ejection Fraction: A Review," *Clin. Ther.*, vol. 37, no. 10, pp. 2186–2198, 2015.
[131] D. W. Kitzman, T. J. O'Neill, and P. H. Brubaker, "Unraveling the Relationship Between Aging and Heart Failure With Preserved Ejection Fraction: The Importance of Exercise and Normative Reference Standards," *JACC Hear. Fail.*, vol. 5, no. 5, pp. 356–358, 2017.
[132] S. V. Brodsky *et al.*, "Prevention and Reversal of Premature Endothelial Cell Senescence and Vasculopathy in Obesity-Induced Diabetes by Ebselen," *Circ. Res.*, vol. 94, no. 3, pp. 377–384, 2004.
[133] R. Kosugi *et al.*, "Angiotensin II receptor antagonist attenuates expression of aging markers in diabetic mouse heart," *Circ. J.*, vol. 70, no. 4, pp. 482–488, 2006.
[134] A. C. Boyd, S. Eshoo, D. A. B. Richards, and L. Thomas, "Hypertension accelerates the 'normal' aging process with a premature increase in left atrial volume," *J. Am. Soc. Hypertens.*, vol. 7, no. 2, pp. 149–156, 2013.
[135] Y. Higashi, Y. Kihara, and K. Noma, "Endothelial dysfunction and hypertension in aging," *Hypertens. Res.*, vol. 35, no. 11, pp. 1039–1047, 2012.
[136] J. P. Coppé *et al.*, "Senescence-associated secretory phenotypes reveal cell-nonautonomous functions of oncogenic RAS and the p53 tumor suppressor.," *PLoS Biol.*, vol. 6, no. 12, 2008.
[137] P. Chang *et al.*, "Swimming exercise inhibits myocardial ER stress in the hearts of aged mice by enhancing cGMP-PKG signaling," *Mol. Med. Rep.*, vol. 21, no. 2, pp. 549–556, 2020.

[138] E. Schulz, T. Jansen, P. Wenzel, A. Daiber, and T. Münzel, “Nitric oxide, tetrahydrobiopterin, oxidative stress, and endothelial dysfunction in hypertension,” *Antioxidants Redox Signal.*, vol. 10, no. 6, pp. 1115–1126, 2008.
[139] D. Drozdz and K. Kawecka-Jaszcz, “Cardiovascular changes during chronic hypertensive states,” *Pediatr. Nephrol.*, vol. 29, no. 9, pp. 1507–1516, 2014.

11 APPENDIX

11.1 Recipes

TNB

1. dilute 0.1M Tris-HCl pH 7.5 + 0.15M NaCl + 0.5% [w/v] TSA Blocking agent [FP1012; Perkin Elmer] in distilled water. Add Blocking Reagent slowly in small increments to buffer while stirring.
2. heat gradually solution for ~1 h to 55°C under continuous stirring
3. store 50mL aliquots at −20°C

Sirius Red

1. dilute 4% [w/v] picric acid (Cat. N. 197378, Sigma Aldrich, Overijse, Belgium) in AD
2. 30' Stirring
3. filter
4. add 0.1% [w/v] old red (Cat. N. 365548, Sigma Aldrich, Overijse, Belgium)
5. stir and filter